EJN fens European Journal of Neuroscience

European Journal of Neuroscience, Vol. 34, pp. 1276–1291, 2011 doi:10.1111/j.1460-9568.2011.07825.x

NEUROSYSTEMS

Computational modelling of 5-HT receptor-mediated reorganization of the brainstem respiratory network

Natalia A. Shevtsova,[1] Till Manzke,[2,3] Yaroslav I. Molkov,[1] Anne Bischoff,[2,3] Jeffrey C. Smith,[4] Ilya A. Rybak[1] and Diethelm W. Richter[2,3]

[1]Department of Neurobiology and Anatomy, Drexel University College of Medicine, Philadelphia, PA, USA
[2]Department of Neuro- and Sensory Physiology, University of Göttingen, Göttingen, Germany
[3]DFG Research Center of Molecular Physiology of the Brain, Göttingen, Germany
[4]Cellular and Systems Neurobiology Section, National Institute of Neurological Disorders and Stroke, National Institutes of Health, Bethesda, MD, USA

Keywords: Bötzinger complex, glycinergic synapses, pre-Bötzinger complex, rescue breathing, respiratory network, serotonin modulation

Abstract

Brainstem respiratory neurons express the glycine α_3 receptor (Glyα_3R), which is a target of modulation by several serotonin (5-HT) receptor agonists. Application of the 5-HT_{1A} receptor (5-HT_{1A}R) agonist 8-OH-DPAT was shown (i) to depress cellular cAMP, leading to dephosphorylation of Glyα_3R and augmentation of postsynaptic inhibition of neurons expressing Glyα_3R (Manzke *et al.*, 2010) and (ii) to hyperpolarize respiratory neurons through 5-HT-activated potassium channels. These processes counteract opioid-induced depression and restore breathing from apnoeas often accompanying pharmacotherapy of pain. The effect is postulated to rely on the enhanced Glyα_3R-mediated inhibition of inhibitory neurons causing disinhibition of their target neurons. To evaluate this proposal and investigate the neural mechanisms involved, an established computational model of the brainstem respiratory network (Smith *et al.*, 2007), was extended by (i) incorporating distinct subpopulations of inhibitory neurons (glycinergic and GABAergic) and their synaptic interconnections within the Bötzinger and pre-Bötzinger complexes and (ii) assigning the 5-HT_{1A}R-Glyα_3R complex to some of these inhibitory neuron types in the network. The modified model was used to simulate the effects of 8-OH-DPAT on the respiratory pattern and was able to realistically reproduce a number of experimentally observed responses, including the shift in the onset of post-inspiratory activity to inspiration and conversion of the eupnoeic three-phase rhythmic pattern into a two-phase pattern lacking the post-inspiratory phase. The model shows how 5-HT_{1A}R activation can produce a disinhibition of inspiratory neurons, leading to the recovery of respiratory rhythm from opioid-induced apnoeas.

Introduction

The respiratory rhythm and motor pattern emerge from a complex combination of intrinsic properties of respiratory neurons and synaptic interactions between them within the respiratory central pattern generator (CPG; Cohen, 1979; Richter, 1982). Various respiratory disturbances that probably arise from perturbations of neuronal excitability and network interactions including complete suppression of breathing (apnoea) are observed during many cardiorespiratory disorders and/or as side-effects of anaesthesia and pharmacological treatments (Boutroy, 1994). Specifically, many pain-relieving drugs include opioids that suppress breathing (Lalley, 2003). Hence, it is important to find pharmacological tools to protect against opioid-induced depression and/or restore breathing during such treatment. After extensive searching several proposals have been made involving activation of different serotonin (5-HT) receptors (Lalley *et al.*, 1997; Richter *et al.*, 1997; Manzke *et al.*, 2009, 2010), which are abundantly expressed in the pre-Bötzinger complex (pre-BötC) and Bötzinger complex (BötC), representing a core of the respiratory CPG (Smith *et al.*, 2007). Activation of the 5-HT IA receptor (5-HT_{1A}R) was most recently found to have therapeutic potential for breathing recovery after opioid-evoked suppression (Sahibzada *et al.*, 2000; Manzke *et al.*, 2010).

This recovery was postulated to originate from an enhanced glycinergic synaptic inhibition associated with the glycinergic α_3 receptor (Glyα_3R) in some inhibitory neurons leading to disinhibition and reactivation of their targets (Manzke *et al.*, 2009, 2010). The underlying mechanisms may involve a complex reorganization of respiratory CPG operation, necessitating analysis of circuit mechanisms that require mathematical or computer modelling for their understanding. The major objectives of this study were (i) to extend our computational model of the respiratory CPG (Smith *et al.*, 2007) to capture experimentally observed effects of opioids and 5-HT_{1A}R activation on respiratory rhythm and pattern and (ii) to use the extended model to propose mechanistic explanations for respiratory

Correspondence: Ilya A. Rybak, as above.
E-mail: rybak@drexel.edu

Received 29 May 2011, revised 7 July 2011, accepted 8 July 2011

network responses to opioids and 5-HT_{1A}R agonists, including the recovery of respiratory rhythm from opioid-induced apnoea.

Our previous computational models of the brainstem respiratory network were able to reproduce many respiratory phenomena (see Rybak *et al.*, 2004a, 2007; Smith *et al.*, 2007; Molkov *et al.*, 2010). The core structure of all these models consisted of interacting populations of excitatory and inhibitory neurons within the pre-BötC and BötC. However, these models did not distinguish between transmitter-specific inhibitory synaptic interactions provided by distinct populations of glycinergic and/or GABAergic respiratory neurons and their modulation by drugs. To consider such synaptic transmission- and receptor-specific interactions, and their modulation, we extended our previous model (Smith *et al.*, 2007) by (i) incorporating distinct subpopulations of glycinergic and GABAergic neurons and specified their synaptic connections in the core network within the BötC and pre-BötC, (ii) assigning the 5-HT_{1A}R-Glyα_3R complex to some neuron types, and (iii) incorporating 5-HT_{1A}R-activated K^+ channels into neurons of the model.

With these modifications, our model reproduced experimentally observed 5-HT_{1A}R-mediated cellular and network responses, and proposes a plausible explanation for rescue of the respiratory rhythm by the 5-HT_{1A}R agonist 8-hydroxy-*N*,*N*-dipropyl-2-aminotetralin (8-OH-DPAT) after opioid-induced apnoea. The model provides new insights into the organization of the respiratory CPG and the modulatory effects of 5-HT and opioids on respiratory network operation.

Materials and methods

The model was developed using as a basis the earlier respiratory CPG model of Smith *et al.* (2007), which described respiratory rhythm generation and pattern formation in mature mammals. In this earlier model, populations of respiratory neurons were defined as either excitatory or inhibitory without distinguishing the inhibitory transmitter types used by different inhibitory populations (see Fig. 1A) and without considering potential mechanisms modulating glycinergic and GABAergic synaptic efficacy in the respiratory network. In the present model we have specified the types of synaptic interactions as excitatory (glutamatergic) or either inhibitory glycinergic or inhibitory GABAergic (as shown in Fig. 1B). Moreover, several key populations of respiratory neurons of the Smith *et al.* (2007) model were split into subpopulations with different connections in the network and/or a different type of postsynaptic receptor-mediated synaptic transmission at their target populations.

All neurons were modelled in the Hodgkin–Huxley style (single-compartment models) and incorporated known biophysical properties and channel kinetics previously characterized in respiratory neurons *in vitro*. Specifically, the kinetics of the fast sodium and the persistent (slowly inactivating) sodium channels were implemented using the experimental data obtained in studies of neurons from the rat rostral ventrolateral medulla (see Rybak *et al.*, 2003a); the kinetics of high-voltage-activated calcium current were described based on the study of calcium currents in rat medullary neurons *in vitro* (Elsen & Ramirez, 1998); the intracellular calcium dynamics were assigned using data by Frermann *et al.* (1999). The descriptions of other ion channels, e.g., the potassium rectifier and calcium-dependent potassium, synaptic conductances, and cellular parameters were as used in our previous models (Rybak *et al.*, 1997a,b, 2003b, 2004a,b). Two additional types of potassium channels were incorporated in the present model. One channel type represented specific K^+ channels activated by the 5-HT_{1A}R agonists such as 8-OH-DPAT, which was added to simulate the hyperpolarizing effect of high doses of 8-OH-DPAT on respiratory neurons (e.g. see Lalley *et al.*, 1994; Manzke *et al.*, 2009). We suggest that these channels are present in all respiratory neurons. The other specific channel type that we suggest is widely present in the respiratory network and was included in all neurons of the model was an opioid-activated inwardly rectifying K^+ (*Kir*) channel (Johnson *et al.*, 1996; Ballanyi *et al.*, 1997, 1999; Takeda *et al.*, 2001; Lalley, 2003). The incorporation of these channels allowed us to simulate the experimentally observed opioid-induced depression of respiratory neuron excitability.

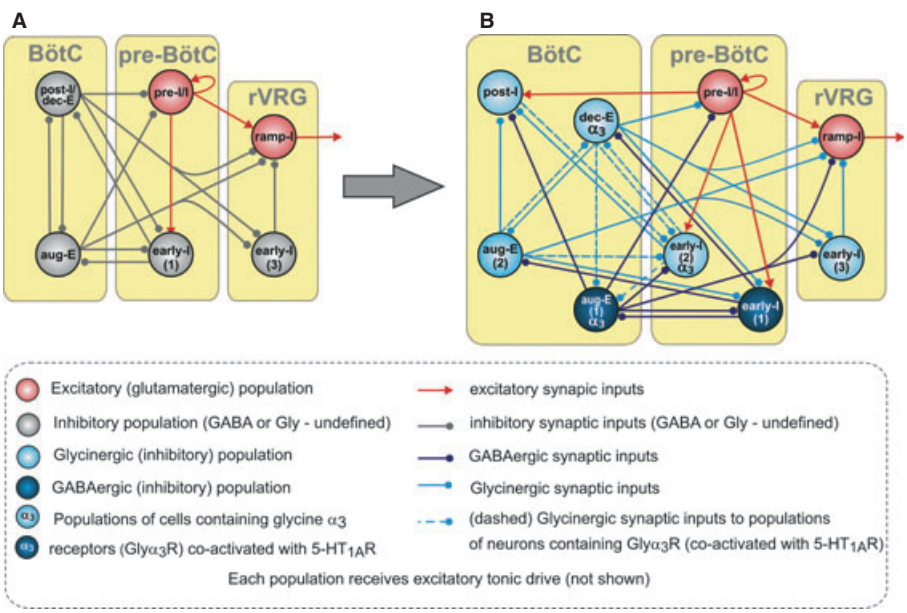

FIG. 1. Schematics of (A) the basic model depicting core components of the brain stem respiratory network distributed within the BötC, pre-BötC and rVRG (modified from Smith *et al.*, 2007 with permission) and (B) the new extended core model proposed in this study. See text and Appendix for full descriptions of model components.

We also postulate that the default postsynaptic glycine receptors mediating glycinergic synaptic inhibition are the α_1 glycine receptors ($Gly\alpha_1R$), and that their operation is independent of 5-HT_{1A}R. In contrast, the $Gly\alpha_3R$ were considered to be present only in selected neuron types receiving glycinergic synaptic inhibition and their additional inhibitory effect required a co-expression of 5-HT_{1A}R. Therefore, the synaptic weights of glycinergic inputs to these selected neurons increased during simulated application of 8-OH-DPAT to produce 5-HT_{1A}R-$Gly\alpha_3$R-dependent potentiation of glycinergic inhibition of these neurons.

Each type of neuron in the model was represented by a population of 20–50 neurons. Heterogeneity of neurons within each population was set by a random distribution of neuronal parameters and initial conditions to produce physiological variations of baseline membrane potential levels, calcium concentrations and channel conductances. Each neural population received an additional tonic excitatory drive.

A full description of the model and its parameters can be found in the Appendix. All simulations were performed using the simulation package NSM 3.0 developed at Drexel University by S. N. Markin, I. A. Rybak and N. A. Shevtsova. Differential equations were solved using the exponential Euler integration method with a step of 0.1 ms. Additional details of the modelling and simulation methods can be found in Rybak *et al.* (2003b, 2007) and Smith *et al.* (2007).

Results

The basic computational model and its extension

Basic model

Our previous computational models of the brainstem respiratory network reproduced many natural and experimentally evoked behaviours observed at the cellular, network and systems levels (see Rybak *et al.,* 2004a; Rybak *et al.*, 2007; Smith *et al.*, 2007; Molkov *et al.*, 2010). These models differed in details incorporated to simulate particular aspects of neural control of breathing, such as the effects of various brainstem transections and vagotomy, effects of various stimulations applied to different nerves and/or neural structures, and perturbations of network activity by metabolic challenges including hypercapnia or hypoxia. All of these previous models, however, had the same core neural circuitry consisting of four populations of respiratory neurons located in the pre-BötC and BötC. This core network includes (i) an excitatory pre-inspiratory/inspiratory (pre-I/I) population of neurons with persistent sodium current-dependent bursting properties and mutual excitatory interactions and (ii) three mutually interacting inhibitory populations: post-inspiratory (post-I) and augmenting-expiratory (aug-E) populations of BötC, and an early-inspiratory [early-I(1)] population of pre-BötC neurons (Fig. 1A; see also Rybak *et al.*, 2007; Smith *et al.*, 2007; Rubin *et al.*, 2009, 2011; Molkov *et al.*, 2010). These models also included an output compartment representing the rostral ventral respiratory group (rVRG) that contained a population of excitatory bulbospinal ramp-inspiratory (ramp-I) neurons, projecting to phrenic motoneurons in the spinal cord, and a population of inhibitory early-I(3) neurons that contributed to shaping the firing pattern of the ramp-I population (Fig. 1A). In addition to mutual synaptic interactions, all neural populations in the model received external excitatory drives simulating inputs from pontine, retrotrapezoid (RTN) and raphé nuclei (not shown in Fig. 1; see Rybak *et al.*, 2004a, 2007; Rubin *et al.*, 2009, 2011; Smith *et al.*, 2007; Molkov *et al.*, 2010). This basic network model is able to generate a three-phase pattern of respiratory activity, originally described by Richter and collaborators (Richter, 1982, 1996; Richter *et al.*, 1986).

Extended model: schematic and operation

The basic model described above did not distinguish between transmitter-specific types of inhibitory synaptic interactions provided by distinct populations of glycinergic and/or GABAergic respiratory neurons, which are known to exist in the respiratory network. Furthermore, neuromodulators such as 5-HT and opioids may differentially affect excitability of the various inhibitory and excitatory neurons depending on neuronal receptors expressed, which can alter network interactions and activity patterns generated. Simulation of such phenomena required modification of the basic model to incorporate different types of synaptic interactions and postsynaptic receptors in the network. In order to consider various transmission- and receptor-specific interactions and their modulation by drugs and neuromodulators, the core network used in our previous models (Fig. 1A) was reorganized and extended as shown in Fig. 1B. Specifically: (i) the population of early-I(1) neurons in the pre-BötC was divided into two populations: a GABAergic early-I(1) and glycinergic early-I(2); (ii) the post-I/decrementing-expiratory (dec-E) population of BötC was split into two separate glycinergic populations: post-I and dec-E with different connectivity within and outside the core circuitry; and (iii) the population of aug-E neurons of BötC was split into separate GABAergic [aug-E(1)] and glycinergic [aug-E(2)] subpopulations.

Thus, as seen in Fig. 1B, the BötC compartment now includes four populations of expiratory inhibitory neurons: the glycinergic post-I and dec-E populations and two aug-E populations, the GABAergic aug-E(1) and the glycinergic aug-E(2). These inhibitory populations provide expiratory inhibition widely distributed within the medullary respiratory network (see Ezure, 1990; Jiang & Lipski, 1990; Tian *et al.*, 1999). In the extended model, the dec-E and each of the aug-E populations inhibit all neurons of the inspiratory populations in the pre-BötC and rVRG [except for the absence of aug-E(2) inhibition of the pre-I/I population], and the post-I population inhibits the early-I(2) population. In addition, we assumed that both aug-E populations inhibit post-I neurons, the aug-E(2) population inhibits dec-E neurons, and the dec-E population inhibits both aug-E populations (Fig. 1B).

Similar to our previous models (Rybak *et al.*, 2007; Smith *et al.*, 2007; Rubin *et al.*, 2009, 2011; Molkov *et al.*, 2010), the pre-I/I population of pre-BötC is the major source of excitatory inspiratory drive in the network and projects to the pre-motor inspiratory ramp-I population of rVRG. The pre-I/I population is composed of mutually interconnected excitatory neurons with persistent sodium current (I_{NaP}) which, under certain conditions (depending on total tonic drive, synaptic inhibition etc.), allows the population to intrinsically generate rhythmic inspiratory activity (Butera *et al.*, 1999a,b; Smith *et al.*, 2000; Rybak *et al.*, 2003b, 2004b) similar to that recorded *in vitro* (Koshiya & Smith, 1999; Johnson *et al.*, 2001) and in the physically reduced neuraxis *in situ* (Smith *et al.*, 2007). However, because of the relatively high excitatory drive (which is considered typical for normal conditions) these neurons operate in a mode in which phasic inhibition provided by the activity of expiratory neurons (aug-E and dec-E) during expiration primarily controls inspiratory burst termination, rather than an I_{NaP}-dependent intrinsic neuronal mechanism (Smith *et al.*, 2007).

All inhibitory neurons in the model [post-I, dec-E, aug-E, early-I(1), early-I(2) and early-I(3)] have intrinsic adapting properties defined by high-voltage activated calcium (Elsen & Ramirez, 1998; Frermann *et al.*, 1999) and calcium-activated potassium currents (Pierrefiche *et al.*, 1999). Because of this, post-I, dec-E, early-I(1), early-I(2) and early-I(3) neurons exhibit decrementing discharge patterns. In contrast, the aug-E neurons, which start firing later in expiration,

exhibit augmenting patterns because of slow disinhibition from the adapting inhibitory dec-E neurons (Richter, 1982). The augmenting activity pattern of the rVRG ramp-I population is shaped by decrementing inhibition from the adapting early-I(3) population (Fig. 1B; Richter, 1982).

Effects of μ-opioids

Despite a long history of studies, the specific cellular and/or network mechanisms underlying respiratory depression (apnoea) produced by μ-opioids are poorly understood. There is experimental evidence that μ-opioid receptors (μ-OR) are widely present in pre-BötC and BötC regions (see Fig. 2G). It has been suggested that opioids activate special potassium inwardly-rectifying (*Kir*)-type channels, hence producing hyperpolarization of pre-BötC and BötC neurons expressing μ-OR (Johnson *et al.*, 1996; Ballanyi *et al.*, 1997, 1999; Takeda *et al.*, 2001; Lalley, 2003). Alternatively, it has been suggested that μ-opioid-induced respiratory depression is mediated by presynaptic inhibition reducing excitatory synaptic inputs to pre-BötC inspiratory neurons (Ballanyi *et al.*, 2009). In our model, we explicitly incorporated postsynaptic μ-OR-activated *Kir* channels (see details in Appendix), and hypothesized that the maximal conductances of these channels in pre-BötC inspiratory neurons are larger than the maximal conductances in BötC expiratory neurons (see Table 2 in the Appendix). Therefore in the model, μ-opioid-induced respiratory depression results from an imbalance of inhibitory interactions between inspiratory and expiratory neurons, resulting in the larger

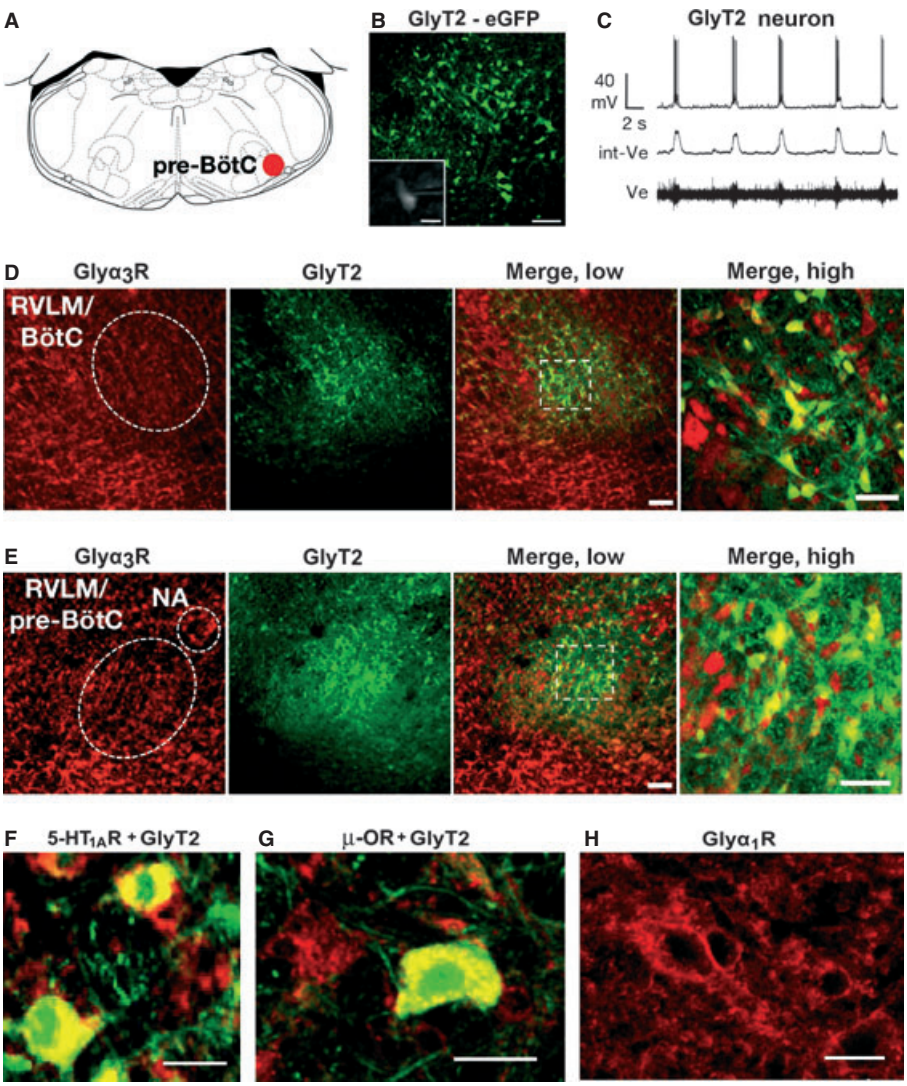

FIG. 2. Immunohistochemical basis for model development. (A) Schematic coronal section of mouse medulla at the level of pre-BötC (red area). (B) Expression of eGFP (enhanced Green Fluorescent Protein) under control of the neuronal GlyT2 (glycine transporter 2) promoter demarcates inhibitory glycinergic neurons (green) within the pre-BötC. (C) Inspiratory activity of glycinergic neurons was identified in medullary slice preparation *in vitro* by rhythmic depolarizations of membrane potential (top trace, obtained by whole-cell recording from eGFP-expressing neuron also visualized by IR-DIC as seen in the B inset); this rhythmic activity correlated with the changes of extracellular field potentials (Ve) recorded from the pre-BötC shown in integrated (middle trace) and raw (bottom trace) signals. (D and E) BötC and pre-BötC glycinergic neurons express $Gly\alpha_3R$. $Gly\alpha_3R$ immunoreactivity ($Gly\alpha_3R$) in the BötC (D, left panel) and pre-BötC (E, left panel). Higher-magnification views of the merged confocal images of $Gly\alpha_3R$ and GlyT2-positive neurons are shown at right. Other abbreviations: RVLM, rostral ventrolateral medulla; NA, nucleus ambiguus. (F) Pre-BötC GlyT2-positive neurons (green) exhibit abundant immunoreactive $5\text{-}HT_{1A}R$ (red and co-expressed with GlyT2 - yellow). (G) Expression of μ-ORs (μ-OR) in the pre-BötC (red and co-expressed with GlyT2 - yellow). (H) Dense $Gly\alpha_1R$ immunoreactivity in the pre-BötC. Figures in all panels, except H are modified from Manzke *et al.* (2010), Figs 1 and 3, with permission, which should be consulted for additional details; H is from unpublished data of T. Manzke and D. W. Richter. Scale bars, 100 μm and 20 μm in inset (A and B), 100 μm (low magnification) and 50 μm (higher magnification) in D and E, 10 μm (F–H).

hyperpolarization (and hence a stronger reduction in excitability) of inspiratory neurons relative to expiratory neurons, which leads to apnoea during which inspiratory neurons become fully inhibited by expiratory neurons.

Glycinergic inhibition and the effects of 5-HT$_{1A}$R agonists

Previous (Sahibzada *et al.*, 2000) and recent (Manzke *et al.*, 2010) findings strongly suggest that activation of 5-HT$_{1A}$R, which are widely expressed in the pre-BötC and BötC regions (Manzke *et al.*, 2009, 2010) promotes recovery of breathing after suppression of respiratory activity by opioids (see Fig. 3A). This recovery was postulated to originate from enhanced glycinergic synaptic inhibition in the pre-BötC and BötC regions (Manzke *et al.*, 2010). The classical Glyα_1R mediating this inhibition is known to be present in these regions (see example in Fig. 2H). In addition, Manzke *et al.* (2010) provided evidence for the expression of Glyα_3R (see Fig. 2D–E) and 5-HT$_{1A}$R (see Fig. 2F) within the pre-BötC and BötC (see Fig. 2A–E). Moreover, application of the 5-HT$_{1A}$R agonist 8-OH-DPAT to wild-type mice was shown to restore respiratory activity from apnoeas caused by systemic application of the μ-OR agonist fentanyl (Fig. 3A). In contrast, breathing in *Glra3*$^{-/-}$ mice containing Glyα_1R but lacking Glyα_3R could not be restored by 5-HT$_{1A}$R stimulation with 8-OH-DPAT (Fig. 3B).

To simulate the specific role of Glyα_3R and its modulation by 5-HT$_{1A}$R activation, we have hypothesized that the dec-E and aug-E(1) neuron populations of BötC and the early-I(2) population of pre-BötC co-express Glyα_3R and 5-HT$_{1A}$R so that activation of 5-HT$_{1A}$R receptors amplifies Glyα_3R-mediated synaptic inhibition of these neurons by other glycinergic neurons (see dashed connections in Fig. 1B). We have also proposed that 8-OH-DPAT can activate, in a concentration-dependent manner, special 5-HT$_{1A}$R-dependent K^+ channels that are assumed to be present in all neurons of the model.

A full description of these features of the model and model parameters are included in the Appendix.

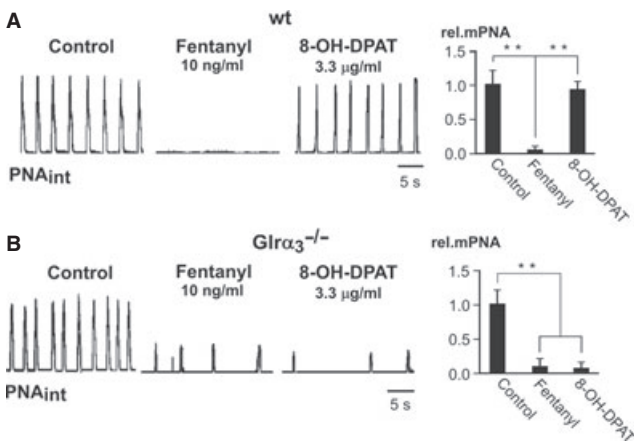

FIG. 3. Effects of 8-OH-DPAT administration on breathing recovery from opioid-induced apnoea in wild and Glr$\alpha_3^{-/-}$ mice. (A) Systemic administration of μ-opioid agonist fentanyl significantly reduced or blocked the phrenic nerve activity (PNA; integrated signals) in arterially perfused mouse brainstem–spinal cord preparations from wild-type (wt) mice, which then recovered after stimulation of 5-HT$_{1A}$R with administration of 8-OH-DPAT via perfusate. (B) The same preparations from Glr$\alpha_3^{-/-}$ mice (lacking Glyα_3R) responded to fentanyl-induced μ-opioid stimulation with respiratory depression that could not be reversed by 5-HT$_{1A}$R stimulation with systemic administration of 8-OH-DPAT. Bar graphs show minute PNA activity relative to control (rel. mPNA, with mPNA calculated as frequency × area of integrated nerve discharges). Data in graphs are mean ± SEM (**$P < 0.01$). Modified from Manzke *et al.* (2010), Fig. 5, with permission.

Model performance under normal conditions

The extended model's performance under normal conditions is shown in Fig. 4A1 and A2. The activity of each neural population (in panel A1) is represented by the average spike frequency histogram of neuron activity. Traces of membrane potential changes of one representative neuron from each population are shown in panel A2. The model generates a typical three-phase respiratory rhythm similar to that generated in the previously described model (see Smith *et al.*, 2007). Note that under normal conditions the two early-I populations of pre-BötC exhibit similar activity profiles, as do both glycinergic and GABAergic aug-E populations of BötC.

Simulation of the effects of 8-OH-DPAT application

Figure 4B1 and B2 shows our simulation of the effects of systemic application of a low dose of a 5-HT$_{1A}$R agonist (8-OH-DPAT). Note that in this simulation we assume that low doses of 8-OH-DPAT do not activate the 5-HT$_{1A}$R-dependent K^+ channels that hyperpolarize respiratory neurons. However, neurons of the early-I(2) population, which have Glyα_3 receptors and receive glycinergic inhibition from the post-I population, are affected by the 5-HT$_{1A}$R modulation of Glyα_3R signalling. The activation of 5-HT$_{1A}$R augments this Glyα_3-mediated inhibition causing complete inhibition of spiking in the early-I(2) population by the glycinergic inputs from the post-I population (Fig. 4B1 and B2, third trace from the top), hence shortening the inspiratory phase. In addition, the post-I neurons are released from inspiratory inhibition and the onset of their activity shifts to the beginning of inspiration (see Fig. 4B1 and B2, fourth trace). As aug-E(1) and dec-E neurons have Glyα_3 receptors, application of 8-OH-DPAT augments both the inhibition of aug-E(1) neurons by the dec-E population and the inhibition of dec-E neurons by the aug-E(2) population. This shortens expiration. As a result, the network starts generating a two-phase rhythm lacking the post-inspiratory phase and the frequency of oscillation increases compared to control.

The results of a simulated application of a higher dose of 8-OH-DPAT are shown in Fig. 4C1 and C2 when simulated neurons undergo activation of 5-HT$_{1A}$R-regulated K^+ channels resulting in a general membrane hyperpolarization. As a result, the pattern of post-I activity transforms into a short late-I discharge at the end of inspiration (see Fig. 4C1 and C2, fourth trace), which causes a further increase in oscillation frequency.

Figure 5B shows the membrane potential of a single post-I neuron in the model under control conditions, after systemic application of a low and higher dose of 8-OH-DPAT, and after recovery as compared with the corresponding intracellular recording from a post-I neuron of anesthetized cat *in vivo* shown in Fig. 5A (from Manzke *et al.*, 2009). It can be seen that after application of 8-OH-DPAT the durations of inspiration and expiration decrease both in the experiment and in our simulation. With a lower dose of 8-OH-DPAT the activity of the post-I neuron shifts to inspiration, whereas with a higher dose the pattern of neuronal activity transforms into a late-I spiking profile associated with significant hyperpolarization of membrane potential (Fig. 5B).

Figure 6B shows the traces of membrane potential of a single model neuron from the aug-E(1) population under control conditions and after simulated local application of a low dose of 8-OH-DPAT to be compared with the corresponding data on the effect of ionophoresis of 8-OH-DPAT to a single aug-E cell in anesthetized cat *in vivo* shown in Fig. 6A (from Richter *et al.*, 1997). In both cases (Fig. 6, panels A and B) activation of neuronal 5-HT$_{1A}$R produced cellular membrane hyperpolarization during both inspiration and post-inspiration (see the

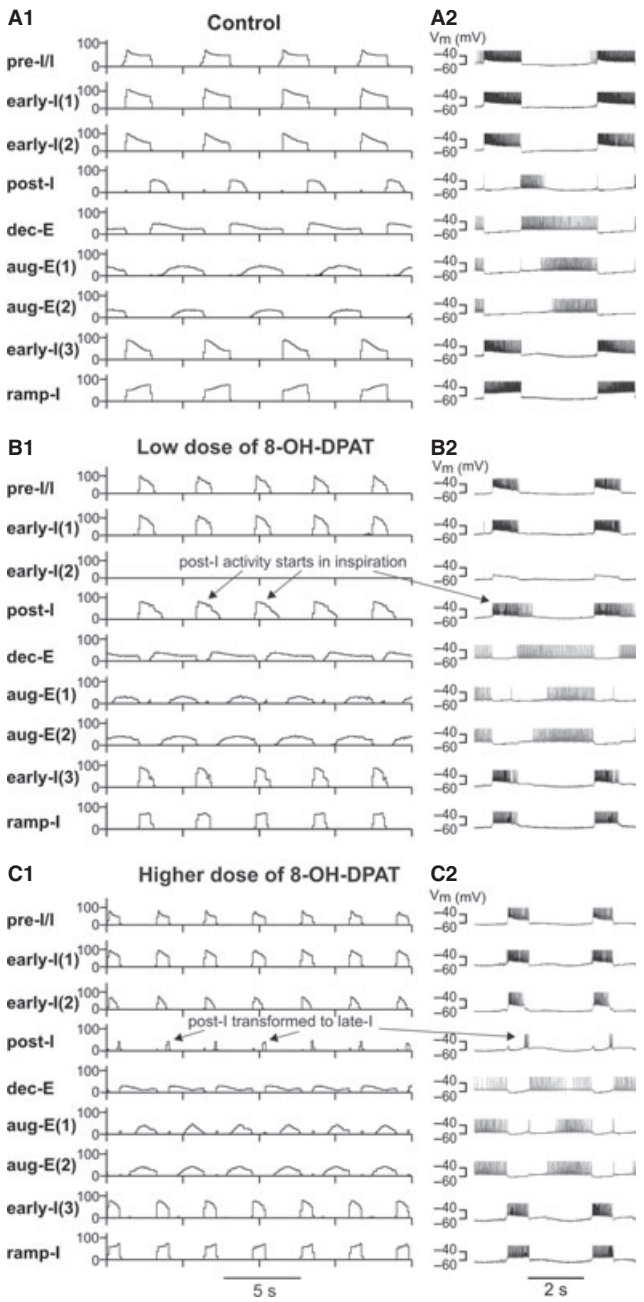

FIG. 4. Model performance under (A1 and A2) simulated control conditions and after application of (B1 and B2) low and (C1 and C2) higher doses of 8-OH-DPAT. In the left panels (A1, B1 and C1), the activity of each population is represented by a histogram of average neuronal spike frequency within population (*y*-axes represent spikes per second per neuron; bin size, 30 ms). In the right panels (A2, B2 and C2), membrane potential traces of one representative neuron from each population are shown at an expanded time scale. Note the shift in onset of activity of post-I neurons to inspiration with a low concentration of applied 8-OH-DPAT (B1 and B2) and the change in their activity to late-I firing profile with a higher drug concentration (C1 and C2).

merged traces on the right). In the simulation, this hyperpolarization results from a 5-HT_{1A}R-Glyα_3R-dependent increase in glycinergic inhibition from the early-I(2) neurons during inspiration and from the glycinergic dec-E neurons during expiration.

An increase in the dose of locally applied 8-OH-DPAT in the model, which activated the special 5-HT_{1A}R-dependent K^+ channels, produced a larger membrane hyperpolarization and a complete suppression of firing in the aug-E cell shown (see Fig. 7B, right trace). This simulation reproduced the changes in the membrane potential and cellular activity shown in Fig. 7A (from Lalley *et al.*, 1994), which represents aug-E cell responses during stronger iontophoresis of 8-OH-DPAT to this cell in anesthetized cat *in vivo*. In our simulation, this additional hyperpolarization was due to the 8-OH-DPAT concentration-dependent activation of the 5-HT_{1A}R -regulated K^+ channels.

A systemic application of 8-OH-DPAT can produce more complicated effects on respiratory neurons because the resultant alterations in cellular behaviour depends on both direct cellular-level changes and the perturbations of synaptic inputs from other neurons whose activity is also affected by the systemically applied drug. This is demonstrated in the simulation of effects of systemic 8-OH-DPAT application on the membrane potential of a single aug-E(1) neuron (Figs 8B and 9B). In contrast to the simulated single-neuron application of 8-OH-DPAT (see Figs 6B and 7B), systematic application of the low drug dose reduced the membrane hyperpolarization (Fig. 8B), which is also seen in the intracellular recordings from aug-E neurons in anesthetized cat (see Fig. 8A from Lalley *et al.*, 1994). From the simulation, the mechanistic explanation for this diminished membrane hyperpolarization is that the systematic application of a low dose of 8-OH-DPAT shifts the post-I activity to inspiration, which suppresses the activity of the glycinergic early-I(2) neurons (see Fig. 4B1 and B2). This also eliminates inhibition of aug-E(1) neurons by early-I(2) neurons (see Fig. 1B), thus significantly reducing the total inhibition of aug-E(1) neurons during inspiration.

With systemic application of higher 8-OH-DPAT doses in the simulation (Fig. 9B), the effects change significantly to an increase in hyperpolarization of aug-E(1) cells during inspiration, which corresponds to that seen in aug-E neurons recorded from anesthetized cat with higher dose of systemically applied drug (see Fig. 9A from Lalley *et al.*, 1994). Our simulation suggests that this larger hyperpolarization may be associated with the conversion of post-I activity to a late-I firing profile. This re-establishes activity of early-I(2) neurons (see Fig. 4C1 and C2) that inhibits aug-E(1) neurons. Furthermore, the activation of K^+ channels at higher drug doses also contributes to the larger hyperpolarization.

Our simulations of the effects on network activity of systemic application of 8-OH-DPAT also predict the perturbations of amplitude and frequency of respiratory motor output. Specifically, Fig. 10 shows how the output activity of the model (as represented by the integrated activity of the ramp-I population) changes with systemic application of low and higher doses of 8-OH-DPAT. It can be seen that the amplitude of the output activity decreases and its frequency increases progressively with drug dose.

Simulation of 8-OH-DPAT-evoked rhythm recovery after opioid-produced depression

Figures 11 shows our simulation of the 8-OH-DPAT-mediated recovery of rhythmic activity after it was completely suppressed by opioids acting through μOR-activated *Kir* channels. In Fig. 11A1 and A2, the excitability of all inspiratory pre-BötC neurons was reduced because of the *Kir* channel activation and they were fully inhibited by the dec-E and two aug-E populations of BötC, which fire tonically in the absence of phasic inhibitory inputs from the pre-BötC inspiratory (early-I) populations. Figure 11B1 and B2, shows the simulation of a subsequent application of a low-dose of 8-OH-DPAT, which augments inhibition of the dec-E and aug-E(1) populations expressing Glyα_3R. This induces disinhibition of pre-I/I and early-I(1) neurons in

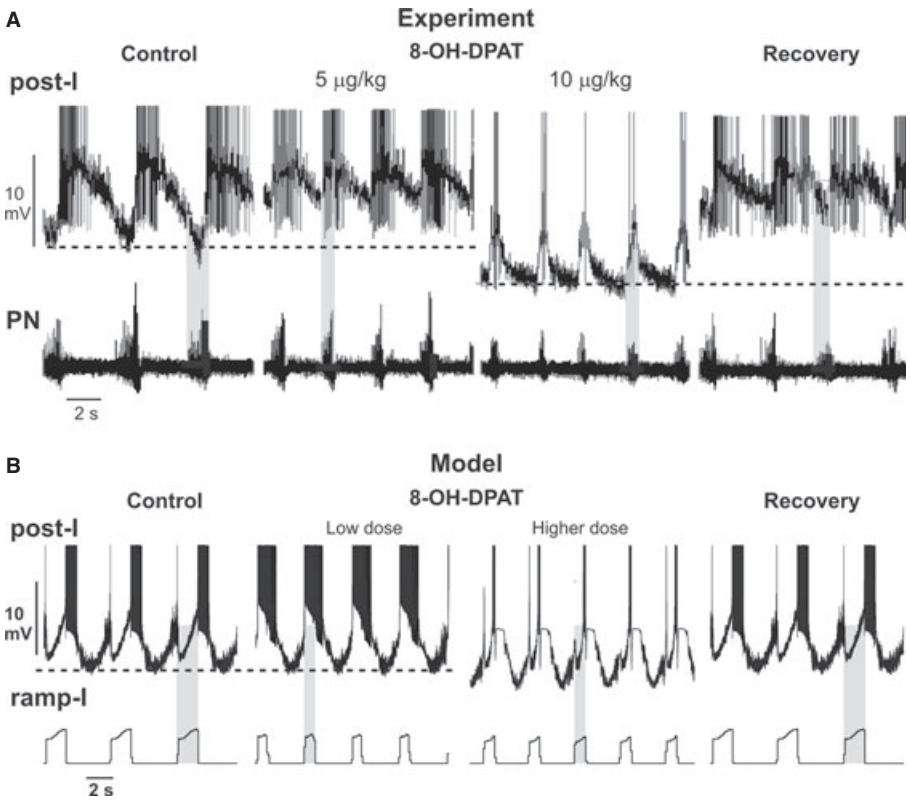

FIG. 5. Changes in the activity of post-I neurons with a systemic 8-OH-DPAT application. (A) The response of post-I neurons recorded within the rVRG in anaesthetized cat *in vivo* to systemic application of the 5-HT_{1A}R agonist 8-OH-DPAT. Post-I neurons normally receive the most powerful synaptic inhibition during inspiration, when phrenic nerves (PN) exhibit an augmenting burst discharge (highlighted in gray). Applying 8-OH-DPAT systemically at low concentrations (5 $\mu g/kg$) induces the release of post-I neurons from inspiratory synaptic inhibition, enabling them to discharge action potentials from the beginning of inspiration (second interval highlighted in gray). At higher concentrations of 8-OH-DPAT (10–50 $\mu g/kg$), post-I neurons hyperpolarize and their action potential firing is limited to the end of inspiratory phase (late-I profile highlighted by gray). From Manzke *et al.*, 2009; Fig. 2 (a), used with permission. (B) Trace of membrane potential of post-I neuron in the model in control conditions, after simulated application of a low and higher dose of 8-OH-DPAT, and after recovery. The bottom trace shows integrated activity of the ramp-I population. See text for details.

the pre-BötC, which restores respiratory oscillations but with a two-phase rhythmic pattern (note that the activity of post-I activity was shifted to inspiration). An expanded view of the corresponding neuronal activities for this case is shown in Fig. 12A.

Figure 11C1 and C2 shows the results in which a simulated higher dose of 8-OH-DPAT restored respiratory oscillations via the combination of 5-HT_{1A}R-mediated potentiation of Glyα_3R and the higher dose-dependent activation of 5-HT_{1A}R-regulated K^+ channels. The corresponding neuronal activities for this case are shown in Fig. 12B.

Figure 13A shows respiratory activity in an *in situ* perfused rat brainstem–spinal cord preparation recorded from the phrenic nerve under control conditions, during subsequent suppression of respiratory activity by the opioid receptor agonist fentanyl, and after recovery of activity by experimental application of 8-OH-DPAT. In Fig. 13B, the integrated activity of the rVRG ramp-I population in the model is shown under corresponding control conditions, during simulated opioid-induced depression, and then after simulated recovery of breathing by low and higher doses of 8-OH-DPAT. Similar to the experimental results, the simulated application of higher doses of the 5-HT_{1A}R agonist produces an increase in the burst frequency and a decrease in burst amplitude of the rVRG bulbospinal ramp-I inspiratory population. Note also that after elimination of Glyα_3 receptors in the model, to simulate the situation in *Glra3*$^{-/-}$ mice lacking Glyα_3R, application of 8-OH-DPAT (any dose) cannot restore the respiratory rhythm after opioid-induced apnoea (see Fig. 13C and compare with Fig. 3B) as in the mutant mice, which indicates a necessary role of Glyα_3 receptors and the 5-HT_{1A}R-mediated Glyα_3R signalling in this recovery of breathing.

Discussion

Extended model architecture and proposed features of respiratory CPG organization

Physiological bases for the extended model

Previous computational models of the respiratory network have not specified different types of transmitter-specific synaptic interactions such as inhibitory glycinergic and GABAergic interactions within the respiratory network. Different types of postsynaptic receptors expressed in different respiratory neuron groups and their possible differential effects on neuronal excitability have also not been considered. However, experimental studies in which specific pharmacological blockers were used (e.g. strychnine to block glycinergic inhibition, or bicuculline, picrotoxin or gabazine to block GABAergic synapses) have clearly demonstrated their different effects on the respiratory rhythm and pattern. Specifically, suppressing glycinergic inhibition in decerebrate cats with strychnine affected mostly late-inspiratory and early-expiratory activity, whereas the GABAergic transmission blocker bicuculline was effective throughout the entire cycle period with a stronger effect during late inspiration (Schmid

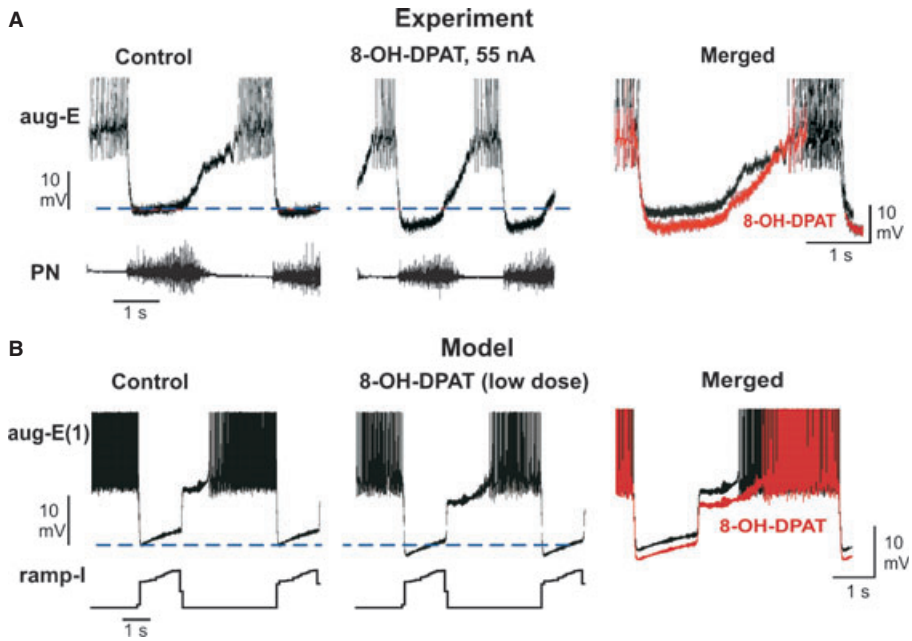

FIG. 6. Effect of local application of 8-OH-DPAT on single aug-E neurons *in vivo* and in the model. (A) Effects of ionophoretic administration of 8-OH-DPAT on membrane potential and discharge properties of an aug-E neuron recorded from anesthetized cat *in vivo* (figure from Richter *et al.*, 1997, used with permission). (B) Simulation results are shown for a single neuron from the aug-E(1) population (GABAergic, with Glyα_3 receptors) with simulated effects of cellular 8-OH-DPAT application (low dose). An increase in membrane hyperpolarization in both cases is illustrated on the right by superposed traces with an expanded time scale. In the simulation, the increase in hyperpolarization results from the Glyα_3-mediated activation-dependent increase in glycinergic inhibition from early-I(2) cells during inspiration and dec-E cells during expiration.

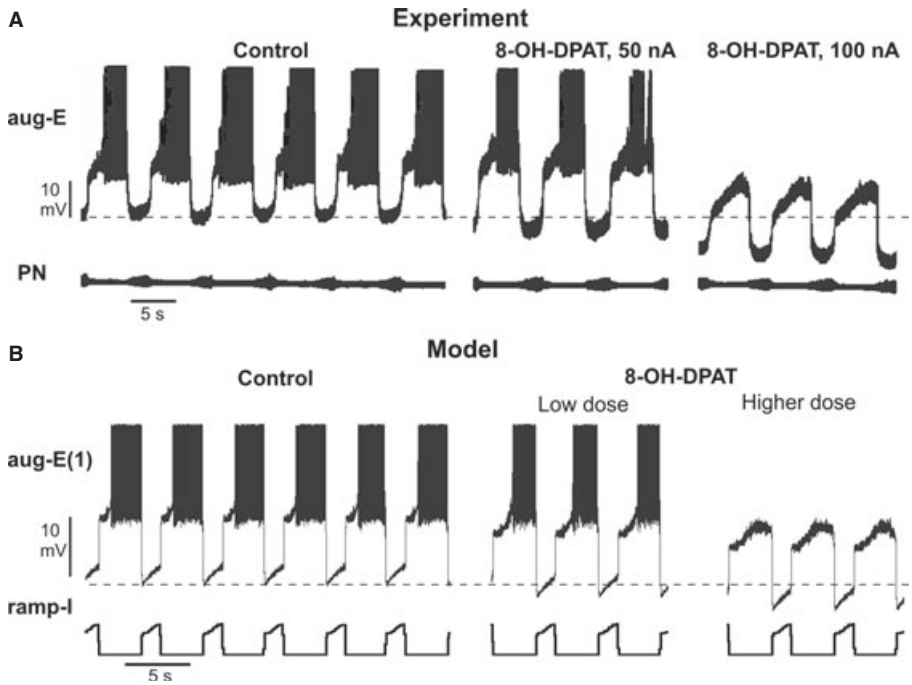

FIG. 7. Effect of an increasing dose of local 8-OH-DPAT application on single aug-E neurons *in vivo* and in the model. (A) Effects of increasing ejected current (ionophoretic administration of 8-OH-DPAT) on the discharge properties of a single aug-E(2) neuron recorded intracellularly in anesthetized cat *in vivo*. Recordings are shown during ionophoresis of 8-OH-DPAT with two different ejecting currents (50 and 100 nA) as indicated. Modified from Lalley *et al.* (1994), Fig. 2, with permission. (B) Simulation results are shown for a single neuron from the aug-E(1) population (GABAergic, with Glyα_3 receptors) affected by simulated cellular 8-OH-DPAT application with low and higher doses. The increase in hyperpolarization and suppression of spiking activity with the higher dose of 8-OH-DPAT in the simulation result from activation of 5-HT$_{1A}$R-regulated K^+ channels in this neuron.

et al., 1996). Bilateral injections of bicuculline (50 or 100 μM) to the pre-BötC of anaesthetized cats slowed respiratory frequency and induced apneustic patterns, whereas bilateral injections of strychnine (50 or 100 μM) to the same region reduced the phrenic burst amplitude and increased burst frequency (Pierrefiche *et al.*, 1998). Pharmacological blockade of glycinergic inhibition in the perfused

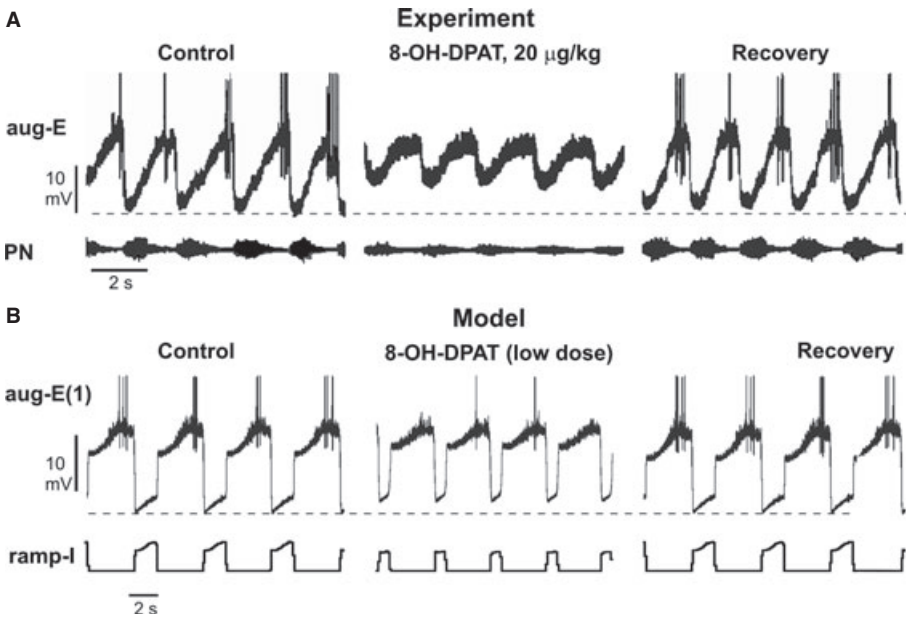

FIG. 8. Effect of systemic application of 8-OH-DPAT on single aug-E neurons. (A) Effects of systemic administration (i.v. injection) of 8-OH-DPAT on the membrane potential of an aug-E neuron and phrenic nerve (PN) activity in anesthetized cat *in vivo*. Dashed line indicates a decreased hyperpolarization during inspiration produced by 8-OH-DPAT (unpublished, from experiments described in Lalley *et al.*, 1994). (B) Simulation of systemic application of a low dose of 8-OH-DPAT is shown for a single neuron from the aug-E(1) population. The reduced hyperpolarization during inspiration produced by 8-OH-DPAT is because a relatively low dose of 8-OH-DPAT shifts the post-I activity to inspiration and suppresses the activity of glycinergic early-I(2) neurons (see Fig. 4B1 and B2). This eliminates inhibition of aug-E(1) neurons by early-I(2) neurons and hence significantly reduces the total inhibition of aug-E(1) neurons during inspiration.

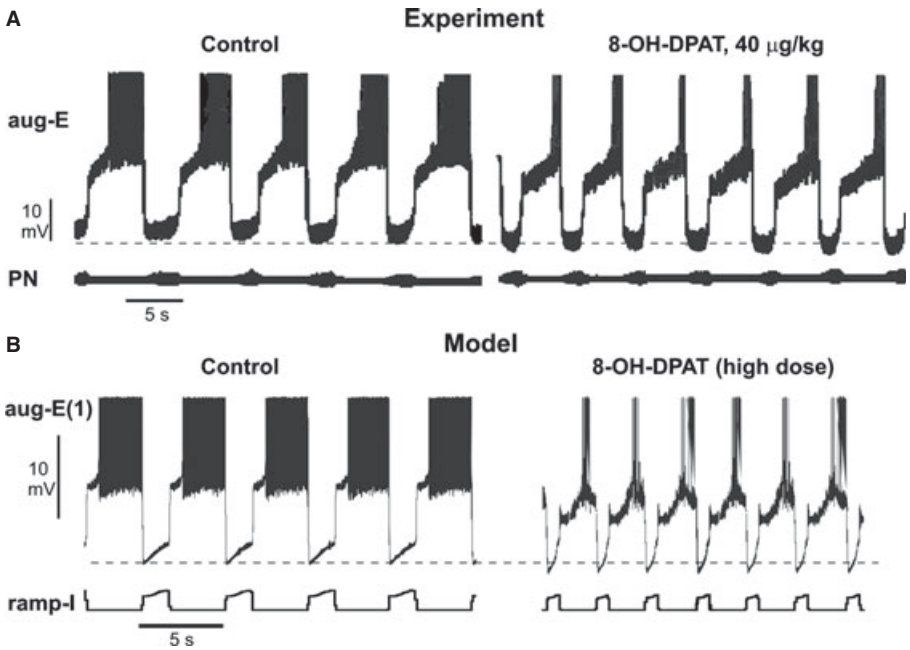

FIG. 9. Effect of systemic application of 8-OH-DPAT on single aug-E neurons. (A) Effects of systemic administration (i.v. injection) of a high dose of 8-OH-DPAT (40 $\mu g/kg$) on the membrane potential of an aug-E neuron and phrenic nerve (PN) activity in anesthetized cat *in vivo*. Dashed line indicates an increase in hyperpolarization during inspiration produced by 8-OH-DPAT. The duration of activity and number of spikes per busts are also reduced by the drug. Modified from Lalley *et al.* (1994), Fig. 1, with permission. (B) Simulation results for systemic application of a high dose of 8-OH-DPAT are shown for a single neuron from the aug-E(1) population. An increase in hyperpolarization and a reduction in spiking activity with the higher dose of 8-OH-DPAT in the simulation result from activation of 5-HT_{1A}R-regulated K^+ channels.

brainstem–spinal cord preparations of adult mice did not stop respiratory oscillations (Büsselberg *et al.*, 2001b). At the same time, it was shown that strychnine application shifted the onset of post-inspiratory activity to inspiration and changed the respiratory pattern from a three-phase cycle to faster, two-phased cycle lacking the post-inspiratory phase (Büsselberg *et al.*, 2001b). Similar two-phase respiratory patterns were observed in mutant oscillator mice lacking glycine receptors (Büsselberg *et al.*, 2001a).

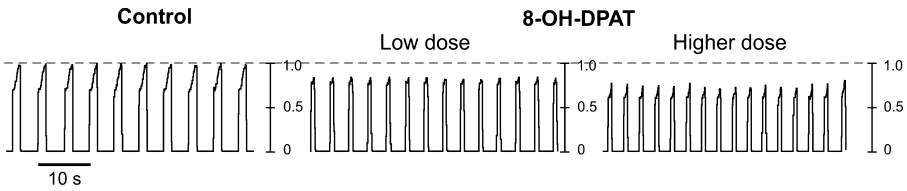

FIG. 10. The output activity of the model (integrated activity of the ramp-I population) under control conditions and after simulated application of a low and higher dose of 8-OH-DPAT.

However, existing data on the transmitter and postsynaptic receptor phenotypes of respiratory neurons are insufficient and in some cases inconsistent. For example, the existence of glycinergic inspiratory neurons in the pre-BötC, such as the inhibitory early-I neurons in our model (see Fig. 1A), has been established (Wang *et al.*, 2001; Winter *et al.*, 2009; Morgado-Valle *et al.*, 2010), but the assumption that all inhibitory neurons in the pre-BötC involved in inspiratory inhibition are glycinergic contradicts the data that inspiratory inhibition in the network persists in mutant oscillator mice lacking functional glycine α_1 receptors, as well as in wild-type mice in which glycinergic inhibition was blocked by administration of strychnine (Büsselberg *et al.*, 2001a,b). The existence of GABAergic inspiratory neurons within the pre-BötC has also been proposed (Onimaru *et al.*, 1990; Brockhaus & Ballanyi, 1998; Liu *et al.*, 2001, 2002) and then directly confirmed by Kuwana *et al.* (2006).

The majority of BötC post-I and/or dec-E neurons with the onset of their activity at the beginning of expiration were characterized as glycinergic (Schmid *et al.*, 1996; Ezure *et al.*, 2003). However, it remains unclear whether the post-I (Richter, 1982; Richter *et al.*, 1986; Schwarzacher *et al.*, 1995) and dec-E (Cohen, 1979; Ezure, 1990; Duffin, 2003) neurons belong to the same population of respiratory neurons (Ezure, 1990; Rybak *et al.*, 1997b); they may represent distinct populations with different connections and functions in the network.

Aug-E neurons are assumed to provide GABAergic inhibition (Champagnat *et al.*, 1982; Haji *et al.*, 1992; Schmid *et al.*, 1996), although glycinergic aug-E neurons in BötC have also been characterized (Schmid *et al.*, 1996; Schreihofer *et al.*, 1999). Expiratory inhibition was found to persist after administration of strychnine and the accompanying shift of post-inspiratory activity to inspiration (Büsselberg *et al.*, 2001b), which implicitly supports the existence of GABAergic aug-E neurons.

Thus, the currently existing data on the possibly different and specific roles of glycinergic and GABAergic inhibition in the core brainstem respiratory network are obviously insufficient for an explicit building of a corresponding computational model. However, these data allow reasonable assumptions concerning differences in the organization of glycinergic and GABAergic inhibition within the respiratory network that, on one hand, do not contradict the existing data described above and, on the other hand, allow reproduction and mechanistic explanation of the specific experimental data on effects of 5-HT_{1A}R agonists on respiratory network performance under different conditions, including the recovery of respiratory activity from opioid-induced depression. To this end the core network used in our previous models (Fig. 1A) was reorganized and extended (Fig. 1B). Importantly, we did not change the general architecture of the respiratory CPG core circuits used in our previous models (Rybak *et al.*, 2007; Smith *et al.*, 2007; see also Fig. 1A), but only elaborated the circuits by defining subpopulations of neurons with different types of inhibitory synaptic transmission and/or postsynaptic transmitter receptors Therefore, the extended model did not lose the ability to reproduce all of the other respiratory responses described previously.

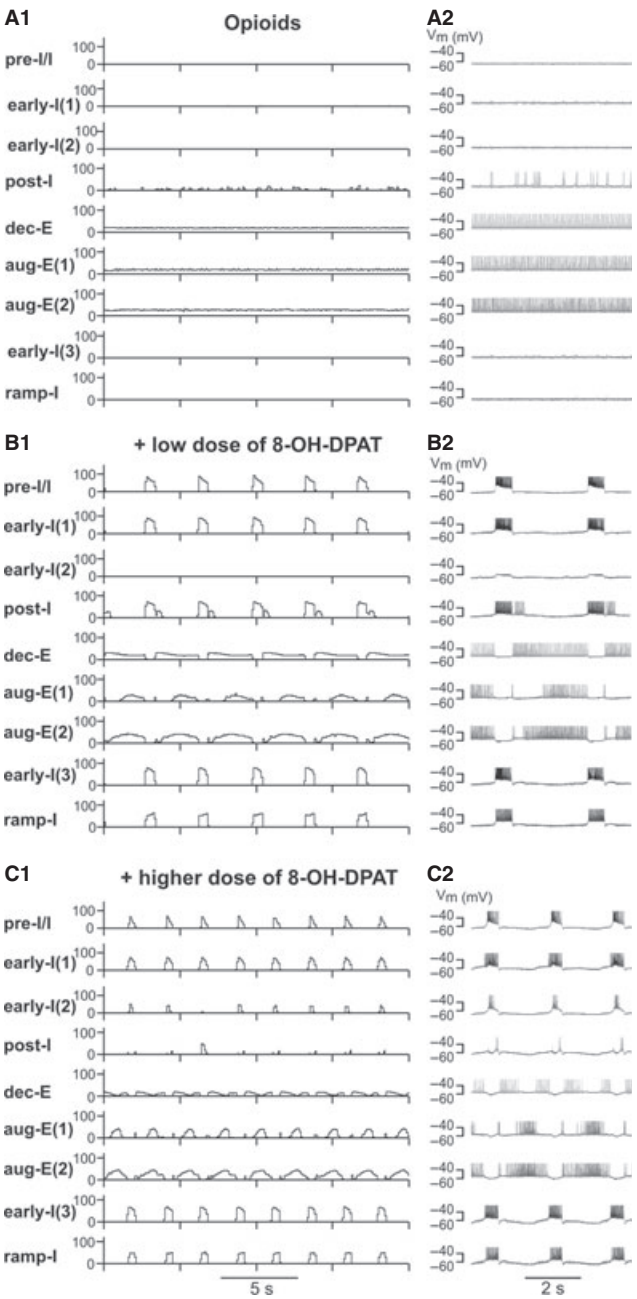

FIG. 11. The model performance after rhythmic activity was suppressed by (A1 and A2) simulated application of opioids and after recovery of rhythmic activity by (B1 and B2) a low and (C1 and C2) a higher dose of 8-OH-DPAT. In the left panels (A1, B1 and C1), the activity of each population is represented by a histogram of average neuronal spike frequency within the population (spikes per second per neuron; bin size, 30 ms). In the right panels (A2, B2 and C2), membrane potential traces of one representative neuron from each population are shown with an expanded time scale.

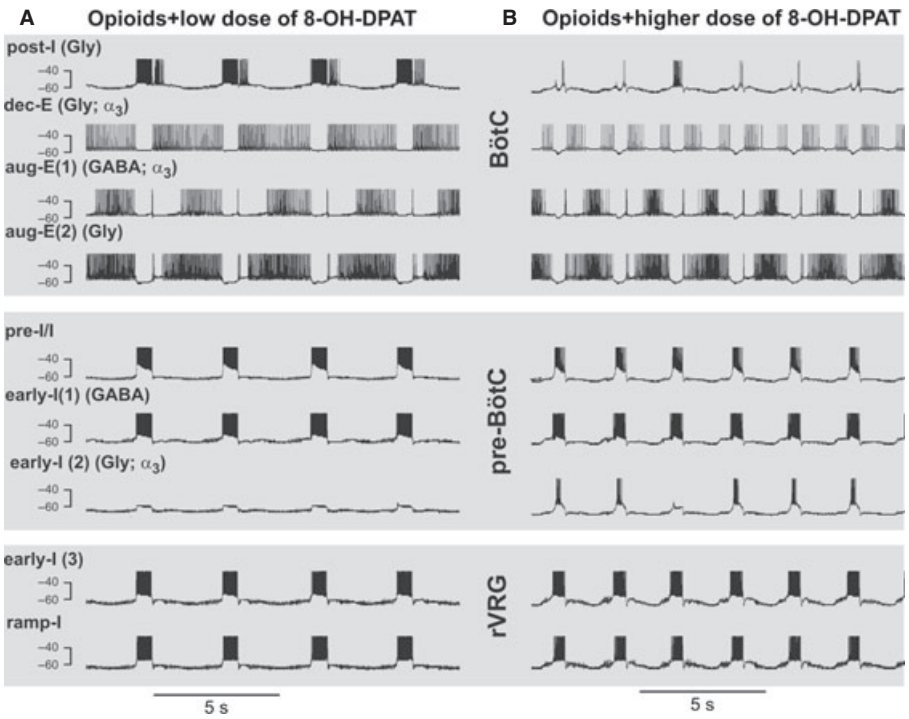

FIG. 12. Expanded view of membrane potentials of single neurons from each population in the model after simulated recovery of the respiratory rhythm with application of (A) a low and (B) a higher dose of 8-OH-DPAT after opioid-induced depression. Inhibitory neurons incorporating Glyα_3R are indicated.

Proposed novel features of respiratory CPG organization

At the same time, the extended model proposes some important details of the respiratory CPG organization that have not been considered previously. Specifically, the present modelling study suggests the following:

1. There are two distinct populations of inhibitory inspiratory neurons in the pre-BötC (termed early-I in our model; see Fig. 1B), one being GABAergic and the other being glycinergic. This proposal eliminates a potential contradiction between the data demonstrating that the pre-BötC inspiratory inhibitory neurons are glycinergic (Wang *et al.*, 2001; Winter *et al.*, 2009; Morgado-Valle *et al.*, 2010) and the data suggesting that these neurons can be GABAergic (Onimaru *et al.*, 1990; Brockhaus & Ballanyi, 1998; Liu *et al.*, 2001, 2002; Kuwana *et al.*, 2006). Furthermore, the model suggests that both of these types of the inhibitory early-I neurons present in the pre-BötC are involved in respiratory rhythmogenesis by providing inhibition of post-I and dec-E as well as aug-E neurons during inspiration. More specifically the GABAergic early-I population [early-I(1) in Fig. 1B] plays an important role in the expiratory–inspiratory transition, while the glycinergic early-I population [early-I(2) in Fig. 1B] seems to be involved in regulation of post-inspiratory activity.
2. There may also be two distinct populations of glycinergic neurons with post-I/dec-E activity patterns (Fig. 1B). One of these populations, the dec-E in Fig. 1B, contains Glyα_3 receptors co-expressed with 5-HT$_{1A}$R. This population contributes significantly to rhythmogenesis, specifically to the inspiratory–expiratory phase transition. The other glycinergic population, the post-I in Fig. 1B, exerts mutually inhibitory interactions with the glycinergic early-I(2) population and is the major source and regulator of post-I activities in the network.
3. There may be two distinct populations of inhibitory aug-E neurons in the BötC (Fig. 1B), one being GABAergic and the other glycinergic. This is consistent with a previous suggestion (Schmid *et al.*, 1996). The model suggests that both of these populations are involved in respiratory rhythmogenesis by providing inhibition of inspiratory neurons during inspiration and of post-I neurons during the late part of expiration.

The evaluation of the current model and its further elaboration will require additional experimental studies including more thorough experimental characterization of the neuronal transmitter-related phenotypes, the corresponding connectivity and the cellular-specific actions of opioids and 5-HT receptor agonists.

Effects of opioids

As noted in the Results section, the mechanisms of respiratory depression (apnoea) produced by μ-opioids are poorly understood. Our current simulations were based on a general depression of neuronal excitability by opioids mediated through activation of potassium channels of the *Kir*-type, which cause hyperpolarization of respiratory (pre-BötC and BötC) neurons (Johnson *et al.*, 1996; Ballanyi *et al.*, 1997, 1999; Takeda *et al.*, 2001; Lalley, 2003). The modelling could be extended to include other potential mechanisms such as opioid-induced presynaptic inhibition that depresses excitatory synaptic inputs to the pre-BötC neurons (Ballanyi *et al.*, 2009) although currently there is limited experimental information on cell-specific changes in synaptic transmission in the network by opioids.

Effects of 5-HT$_{1A}$R agonists and recovery from opioid-induced apnoea

The present computational modelling was able to simulate the effects of the 5-HT$_{1A}$R agonist 8-OH-DPAT on the respiratory rhythm and pattern, including reproducing changes in the activity of specific

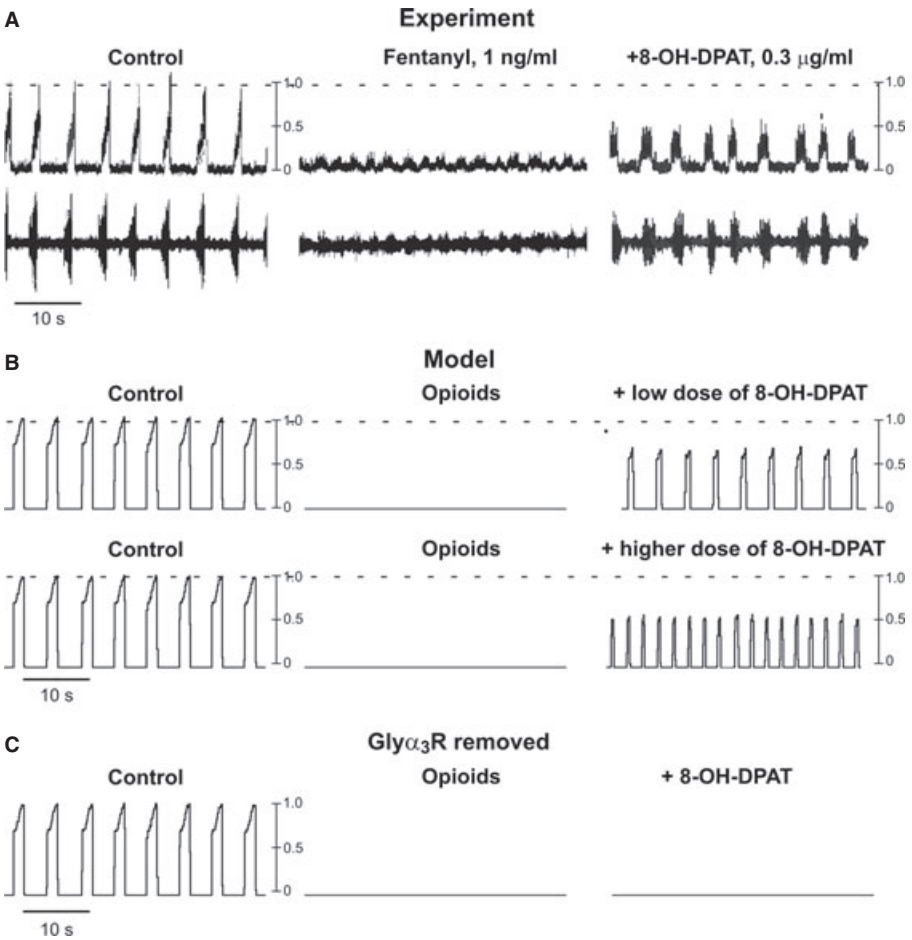

FIG. 13. Suppression of respiratory oscillations by the μ-opioid agonist fentanyl followed by their recovery by 8-OH-DPAT application. (A) Recordings from an *in situ* perfused rat brainstem–spinal cord preparation (bottom trace, raw recording; top trace, integrated phrenic nerve activity; unpublished data from the experiments described in Guenther *et al.*, 2009). (B) Simulation of rhythm suppression followed by its recovery with application of (top) low and (bottom) higher doses of 8-OH-DPAT. The integrated activity of the ramp-I population only is shown. Note that the restored activity is characterized by higher frequency and lower amplitude than control. (C) Simulation shows that after removal of Glyα_3 receptors in the model, application of 8-OH-DPAT (any dose) cannot restore the respiratory rhythm after opioid-induced apnoea. This is consistent with a necessary role of Glyα_3 receptors and 5-HT$_{1A}$R-Glyα_3R signalling in restoration of breathing as obtained in *Glra3*$^{-/-}$ mice lacking Glyα_3R (see Fig. 3B).

respiratory neurons as well as the respiratory recovery from opioid-induced apnoeas. These simulations reproduced the experimentally observed shift in the onset of post-I activity to inspiration and the associated conversion of the three-phase respiratory pattern to a two-phase pattern lacking the post-I phase resulting from a low dose of 8-OH-DPAT (Figs 4B1 and B2, and 5A and B). The model also reproduced the conversion of post-I activity profiles to a late-I spiking pattern accompanied by an increase in the phrenic nerve (PN) discharge frequency and a decrease in the PN amplitude as seen experimentally with higher doses of 8-OH-DPAT (Figs 4C1 and C2, and 5A and B). We were also able to replicate a series of experimental data on the effects of local and systemic applications of low and higher doses of 8-OH-DPAT on the activity of aug-E neurons (Figs 6–9). Changes in the firing patterns of other neuron types produced by the model can be considered model predictions for further experimental studies.

Our model suggests two possible mechanisms contributing to the recovery of respiratory activity from opioid-induced apnoea depending on the low vs. higher dose of 8-OH-DPAT. As described above, opioids strongly reduce the excitability of pre-BötC inspiratory neurons, hence causing an imbalance in mutual inhibition between inspiratory and expiratory neurons. As a result, application of opioids leads to an expiratory activity-related apnoea, in which some expiratory populations (dec-E and both aug-E populations in Fig. 11A1 and A2) become tonically active and inhibit all inspiratory neurons. Application of the 8-OH-DPAT causes activation of glycinergic α_3 receptors (Glyα_3R) present in the glycinergic populations of dec-E and early-I(2) neurons and also in the GABAergic aug-E population (see Fig. 1B). This is consistent with the description that these receptors are widely distributed in the pre-BötC and BötC (Manzke *et al.*, 2009, 2010; see also Fig. 2D and E). Activation of the 5-HT$_{1A}$R-modulated Glyα_3R signalling pathway significantly increases the efficacy of glycinergic synaptic inhibition to these neurons (i.e., increases the glycinergic IPSPs; Manzke *et al.*, 2009, 2010). According to our schematic (Fig. 1B), this specifically amplifies the inhibitory input from aug-E(2) neurons to the dec-E neurons and from dec-E neurons to aug-E(1) neurons, to finally disinhibit the inspiratory neurons. Augmented inhibition of the early-I(2) population by the glycinergic post-I population leads to disinhibition of the latter population during inspiration. As a result, a respiratory rhythm with a two-phase activity pattern recovers from the apnoea with the post-I neurons being active during inspiration (see Fig. 11B1 and B2).

The second mechanism contributing to the respiratory recovery proposed by the model becomes effective when the dose of applied 8-OH-DPAT is high enough to activate the specific 5-HT$_{1A}$R-

regulated K^+ channels, which induces neuronal membrane hyperpolarization depending on the maximal conductance (density) of these channels in each neuron type. According to the model, this neuron type-specific hyperpolarization may serve as an additional mechanism for compensation of the opioid-induced imbalance between mutually inhibiting expiratory and inspiratory neurons, leading to the recovery of respiratory oscillations (see Fig. 11C1 and C2).

The neural mechanisms described above require a respiratory neuron type-dependent distribution of $Gly\alpha_3R$ in the respiratory network; this has no experimental evidence so far and is currently our hypothesis. Our model also suggests that specific $5\text{-}HT_{1A}R$-activated K^+ channels, causing a $5\text{-}HT_{1A}R$-dependent hyperpolarization, exist in all respiratory neurons. Such hyperpolarization has been so far tested and observed only in the post-I (Manzke *et al.*, 2009; see Fig. 5A) and aug-E (or E2, Lalley *et al.*, 1994; see Fig. 7A) neuron types. However, it has been suggested that the activation effect of $5\text{-}HT_{1A}R$ on such K^+ channels is mediated by cyclic AMP (cAMP, e.g. see Richter *et al.*, 1997; Heine *et al.*, 2002) and hence may take place in many or even all types of respiratory neurons. Also, the respiratory neuron-specific actions of $5\text{-}HT_{1A}R$ and μ-OR agonists within the respiratory network have not been adequately established.

Nevertheless, the two mechanisms described above, suggested and tested with our model, propose a reasonable explanation for the experimentally observed $5\text{-}HT_{1A}R$-dependent recovery of the respiratory rhythm from opioid-induced apnoeas. Further coordinated experimental studies are necessary to evaluate our modelling predictions and understand the exact mechanisms of opioid and 5-HT receptor-mediated control of respiratory CPG operation under different physiological and pathophysiological conditions.

Acknowledgements

This study was supported in the USA by NIH grants R01 NS057815, R01 NS069220 and R33 HL087379, and in part by the Intramural Research Program of the NIH, NINDS, and in Germany by the DFG Research Center 'Molecular physiology of the brain'.

Abbreviations

μ-OR, μ-opioid receptor; 5-HT, serotonin; $5\text{-}HT_{1A}R$, 1A 5-HT receptor; 8-OH-DPAT, 8-hydroxy-*N*,*N*-dipropyl-2-aminotetralin; aug-E, augmenting-expiratory (neuron); BötC, Bötzinger complex; CPG, central pattern generator; dec-E, decrementing-expiratory (neuron); early-I, early-inspiratory (neuron); $Gly\alpha_1R$, α_1 glycine receptors; $Gly\alpha_3R$, glycinergic α_3 receptor; $Gly\alpha_3R$, α_3 glycine receptor; I_{CaL}, high-voltage-activated calcium current; $I_{K,Ca}$, calcium-activated potassium current; I_{NaP}, persistent sodium current; *Kir* channel, inwardly rectifying K^+ channel; *Kir*, potassium inwardly-rectifying (channel); post-I, post-inspiratory (neuron); pre-BötC, pre-Bötzinger complex; pre-I/I, pre-inspiratory/inspiratory (neuron); ramp-I, ramp-inspiratory (neuron); RTN, retrotrapezoid nucleus; rVRG, rostral ventral respiratory group.

References

Ballanyi, K., Lalley, P.M., Hoch, B. & Richter, D.W. (1997) cAMP-dependent reversal of opioid- and prostaglandinmediated depression of the isolated respiratory network in newborn rats. *J. Physiol.*, **504**, 127–134.

Ballanyi, K., Onimaru, H. & Homma, I. (1999) Respiratory network function in the isolated brainstem-spinal cord of newborn rats. *Prog. Neurobiol.*, **59**, 583–634.

Ballanyi, K., Ruangkittisakul, A. & Onimaru, H. (2009) Opioids prolong and anoxia shortens delay between onset of preinspiratory (pFRG) and inspiratory (preBötC) network bursting in newborn rat brainstems. *Pflügers Arch.*, **458**, 571–587.

Boutroy, M.J. (1994) Drug-induced apnea. *Biol. Neonate*, **65**, 252–257.

Brockhaus, J. & Ballanyi, K. (1998) Synaptic inhibition in the isolated respiratory network of neonatal rats. *Eur. J. Neurosci.*, **10**, 3823–3839.

Büsselberg, D., Bischoff, A.M., Becker, K., Becker, C.M. & Richter, D.W. (2001a) The respiratory rhythm in mutant oscillator mice. *Neurosci. Lett.*, **316**, 99–102.

Büsselberg, D., Bischoff, A.M. & Paton, J.F.R. (2001b) Reorganization of respiratory network activity after loss of glycinergic inhibition. *Pflügers Arch.*, **441**, 444–449.

Butera, R.J., Rinzel, J. & Smith, J.C. (1999a) Models of respiratory rhythm generation in the pre-Bötzinger complex. I. Bursting pacemaker neurons. *J. Neurophysiol.*, **82**, 382–397.

Butera, R.J., Rinzel, J.R. & Smith, J.C. (1999b) Models of respiratory rhythm generation in the pre-Bötzinger complex: II. Populations of coupled pacemaker neurons. *J. Neurophysiol.*, **82**, 398–415.

Champagnat, J., Denavit-Saubie, M., Moyanova, S. & Rondouin, G. (1982) Involvement of amino acids in periodic inhibitions of bulbar respiratory neurones. *Brain Res.*, **237**, 351–365.

Cohen, M.I. (1979) Neurogenesis of respiratory rhythm in the mammal. *Physiol. Rev.*, **59**, 1105–1173.

Duffin, J. (2003) A commentary on eupnoea and gasping. *Respir. Physiol. Neurobiol.*, **139**, 105–111.

Elsen, F.P. & Ramirez, J.M. (1998) Calcium currents of rhythmic neurons recorded in the isolated respiratory network of neonatal mice. *J. Neurosci.*, **18**, 10652–10662.

Ezure, K. (1990) Synaptic connections between medullary respiratory neurons and considerations on the genesis of respiratory rhythm. *Prog. Neurobiol.*, **35**, 429–450.

Ezure, K., Tanaka, I. & Kondo, M. (2003) Glycine is used as a transmitter by decrementing expiratory neurons of the ventrolateral medulla in the rat. *J. Neurosci.*, **23**, 8941–8948.

Frermann, D., Keller, B.U. & Richter, D.W. (1999) Calcium oscillations in rhythmically active respiratory neurones in the brain stem of the mouse. *J. Physiol.*, **515**, 119–131.

Guenther, U., Manzke, T., Wrigge, H., Dutschmann, M., Zinserling, J., Putensen, C. & Hoeft, A. (2009) *Anesth. Analg.*, **108**, 1169–1176.

Haji, A., Takeda, R. & Remmers, J.E. (1992) Evidence that glycine and GABA mediate postsynaptic inhibition of bulbar respiratory neurons in the cat. *J. Appl. Physiol.*, **73**, 2333–2342.

Heine, M., Ponimaskin, E., Bickmeyer, U. & Richter, D.W. (2002) 5-HT-receptor-induced changes of the intracellular cAMP level monitored by a hyperpolarization-activated cation channel. *Pflügers Arch.*, **443**, 418–426.

Jiang, C. & Lipski, J. (1990) Extensive monosynaptic inhibition of ventral respiratory group neurons by augmenting neurons in the Bötzinger complex in the cat. *Exp. Brain Res.*, **81**, 639–648.

Johnson, S.M., Smith, J.C. & Feldman, J.L. (1996) Modulation of respiratory rhythm in vitro: role of Gi/o protein-mediated mechanisms *J. Appl. Physiol.*, **80**, 6–2120.

Johnson, S.M., Koshiya, N. & Smith, J.C. (2001) Isolation of the kernel for respiratory rhythm generation in a novel preparation: the pre-Bötzinger complex ''island''. *J. Neurophysiol.*, **85**, 1772–1776.

Koshiya, N. & Smith, J.C. (1999) Neuronal pacemaker for breathing visualized in vitro. *Nature*, **400**, 360–363.

Kuwana, S., Tsunekawa, N., Yanagawa, Y., Okada, Y., Kuribayashi, J. & Obata, K. (2006) Electrophysiological and morphological characteristics of GABAergic respiratory neurons in the mouse pre-Bötzinger complex. *Eur. J. Neurosci.*, **23**, 667–674.

Lalley, P.M. (2003) μ-Opioid receptor agonist effects on medullary respiratory neurons in the cat: evidence for involvement in certain types of ventilatory disturbances. *Am. J. Physiol. Regul. Integr. Comp. Physiol.*, **285**, R1287–R1304.

Lalley, P.M., Bischoff, A.M. & Richter, D.W. (1994) 5-HT-1A receptor-mediated modulation of medullary expiratory neurones in the cat. *J. Physiol.*, **476**, 117–130.

Lalley, P.M., Pierrefiche, O., Bischoff, A.M. & Richter, D.W. (1997) cAMP-dependent protein kinase modulates expiratory neurons in vivo. *J. Neurophysiol.*, **77**, 1119–1131.

Liu, Y.Y., Ju, G. & Wong-Riley, M.T. (2001) Distribution and colocalization of neurotransmitters and receptors in the pre-Bötzinger complex of rats. *J. Appl. Physiol.*, **91**, 1387–1395.

Liu, Y.Y., Wong-Riley, M.T., Liu, J.P., Jia, Y., Liu, H.L., Jiao, X.Y. & Ju, G. (2002) GABAergic and glycinergic synapses onto neurokinin-1 receptor immunoreactive neurons in the pre-Bötzinger complex of rats: light and electronmicroscopic studies. *Eur. J. Neurosci.*, **16**, 1058–1066.

Manzke, T., Dutschmann, M., Schlaf, G., Mörschel, M., Koch, U.R., Ponimaskin, E., Bidon, O., Lalley, P.M.&. & Richter, D.W. (2009) Serotonin targets inhibitory synapses to induce modulation of network functions. *Phil. Trans. R. Soc. B*, **364**, 2589–2602.

Manzke, T., Niebert, M., Koch, U.R., Caley, A., Vogelgesang, S., Hülsmann, S., Ponimaskin, E., Müller, U., Smart, T.G., Harvey, R.J. & Richter, D.W. (2010) Serotonin receptor 1A-modulated phosphorylation of glycine receptor α3 controls breathing in mice. *J. Clin. Invest.*, **120**, 4118–4128.
Molkov, Y.I., Abdala, A.P.L., Bacak, B.J., Smith, J.C., Paton, J.F.R. & Rybak, I.A. (2010) Late-expiratory activity: emergence and interactions with the respiratory CPG. *J. Neurophysiol.*, **104**, 2713–2729.
Morgado-Valle, C., Baca, S.M. & Feldman, J.L. (2010) Glycinergic pacemaker neurons in preBötzinger Complex of neonatal mouse. *J. Neurosci.*, **30**, 3634–3639.
Onimaru, H., Arata, A. & Homma, I. (1990) Inhibitory synaptic inputs to the respiratory rhythm generator in the medulla isolated from newborn rats. *Pflügers Arch.*, **417**, 425–432.
Pierrefiche, O., Schwarzacher, S.W., Bischoff, A.M. & Richter, D.W. (1998) Blockade of synaptic inhibition within the pre-Bötzinger complex in the cat suppresses respiratory rhythm generation in vivo. *J. Physiol.*, **509**, 245–254.
Pierrefiche, O., Haji, A., Bischoff, A. & Richter, D.W. (1999) Calcium currents in respiratory neurons of the cat in vivo. *Pflugers Arch.*, **438**, 817–826.
Richter, D.W. (1982) Generation and maintenance of the respiratory rhythm. *J. Exp. Biol.*, **100**, 93–107.
Richter, D.W. (1996) Neural regulation of respiration: rhythmogenesis and afferent control. In Gregor, R. & Windhorst, U. (Eds), *Comprehensive Human Physiology*. Springer-Verlag, Berlin, Vol. **2**, pp. 2079–2095.
Richter, D.W., Ballantyne, D. & Remmers, J.E. (1986) How is the respiratory rhythm generated? A model *News Physiol. Sci.*, **1**, 109–112.
Richter, D.W., Lalley, P.M., Pierrefiche, O., Haji, A., Bischoff, A.M., Wilken, B. & Hanefeld, F. (1997) Intracellular signal pathways controlling respiratory neurons. *Respir. Physiol.*, **110**, 113–123.
Rubin, J.E., Shevtsova, N.A., Ermentrout, G.B., Smith, J.C. & Rybak, I.A. (2009) Multiple rhythmic states in a model of the respiratory central pattern generator. *J. Neurophysiol.*, **101**, 2146–2165.
Rubin, J.E., Bacak, B.J., Molkov, Y.I., Shevtsova, N.A., Smith, J.C. & Rybak, I.A. (2011) Interacting oscillations in neural control of breathing: modeling and qualitative analysis. *J. Comput. Neurosci.*, **30**, 607–632.
Rybak, I.A., Paton, J.F.R. & Schwaber, J.S. (1997a) Modeling neural mechanisms for genesis of respiratory rhythm and pattern: I. Models of respiratory neurons. *J. Neurophysiol.*, **77**, 1994–2006.
Rybak, I.A., Paton, J.F.R. & Schwaber, J.S. (1997b) Modeling neural mechanisms for genesis of respiratory rhythm and pattern: II. Network models of the central respiratory pattern generator. *J. Neurophysiol.*, **77**, 2007–2026.
Rybak, I.A., Ptak, K., Shevtsova, N.A. & McCrimmon, D.R. (2003a) Sodium currents in neurons from the rostroventrolateral medulla of the rat. *J. Neurophysiol.*, **90**, 1635–1642.
Rybak, I.A., Shevtsova, N.A., St-John, W.M., Paton, J.F. & Pierrefiche, O. (2003b) Endogenous rhythm generation in the pre-Bötzinger complex and ionic currents: modelling and in vitro studies. *Eur. J. Neurosci.*, **18**, 239–257.
Rybak, I.A., Shevtsova, N.A., Paton, J.F., Dick, T.E., St-John, W.M., Morschel, M. & Dutschmann, M. (2004a) Modeling the ponto-medullary respiratory network. *Respir. Physiol. Neurobiol.*, **143**, 307–319.
Rybak, I.A., Shevtsova, N.A., Ptak, K. & McCrimmon, D.R. (2004b) Intrinsic bursting activity in the pre-Bötzinger Complex: role of persistent sodium and potassium currents. *Biol. Cybern.*, **90**, 59–74.
Rybak, I.A., Abdala, A.P., Markin, S.N., Paton, J.F. & Smith, J.C. (2007) Spatial organization and state-dependent mechanisms for respiratory rhythm and pattern generation. *Prog. Brain Res.*, **165**, 201–220.
Sahibzada, N., Ferreira, M., Wasserman, A.M., Taveira- DaSilva, A.M. & Gillis, R.A. (2000) Reversal of morphine-induced apnea in the anesthetized rat by drugs that activate 5-hydroxytryptamine(1A) receptors. *J. Pharmacol. Exp. Ther.*, **292**, 704–713.
Schmid, K., Foutz, A.S. & Denavit-Saubie, M. (1996) Inhibitions mediated by glycine and GABAA receptors shape the discharge pattern of bulbar respiratory neurons. *Brain Res.*, **710**, 150–160.
Schreihofer, A.M., Stornetta, R.L. & Guyenet, P.G. (1999) Evidence for glycinergic respiratory neurons: Bötzinger neurons express mRNA for glycinergic transporter 2. *J. Comp. Neurol.*, **407**, 583–597.
Schwarzacher, S.W., Smith, J.C. & Richter, D.W. (1995) Pre-Bötzinger complex in the cat. *J. Neurophysiol.*, **73**, 1452–1461.
Smith, J.C., Butera, R.J., Koshiya, N., Del Negro, C., Wilson, C.G. & Johnson, S.M. (2000) Respiratory rhythm generation in neonatal and adult mammals: the hybrid pacemaker-network model. *Respir. Physiol.*, **122**, 131–147.
Smith, J.C., Abdala, A.P., Koizumi, H., Rybak, I.A. & Paton, J.F. (2007) Spatial and functional architecture of the mammalian brain stem respiratory network: a hierarchy of three oscillatory mechanisms. *J. Neurophysiol.*, **98**, 3370–3387.
Takeda, S., Eriksson, L.I., Yamamoto, Y., Joensen, H., Onimaru, H. & Lindahl, S.G. (2001) Opioid action on respiratory neuron activity of the isolated respiratory network in newborn rats. *Anesthesiology*, **95**, 740–749.
Tian, G.F., Peever, J.H. & Duffin, J. (1999) Bötzinger-complex, bulbospinal expiratory neurones monosynaptically inhibit ventral-group respiratory neurones in the decerebrate rat. *Exp. Brain Res.*, **124**, 173–180.
Wang, H., Stornetta, R.L., Rosin, D.L. & Guyenet, P.G. (2001) Neurokinin-1 receptor-immunoreactive neurons of the ventral respiratory group in the rat. *J. Comp. Neurol.*, **434**, 128–146.
Winter, S.M., Fresemann, J., Schnell, C., Oku, Y., Hirrlinger, J. & Hülsmann, S. (2009) Glycinergic interneurons are functionally integrated into the inspiratory network of mouse medullary slices. *Pflugers Arch.*, **458**, 459–469.

Appendix

Single neuron descriptions

All neurons were modelled in the Hodgkin–Huxley style as single-compartment models:

$$C \cdot \frac{dV}{dt} = -I_{Na} - I_{NaP} - I_K - I_{CaL} - I_{K,Ca} - I_L - I_{Kir} - I_{KS} - I_{SynE} - I_{Syn\_GABA} - I_{Syn\_GLY}, \quad (1)$$

where V is the membrane potential, C is the membrane capacitance and t is time. The terms in the right part of this equation represent ionic currents: I_{Na}, fast sodium (with maximal conductance $\bar{g}_{Na}$); I_{NaP}, persistent (slowly inactivating) sodium (with maximal conductance $\bar{g}_{NaP}$); I_K, delayed-rectifier potassium (with maximal conductance $\bar{g}_K$); I_{CaL}, high-voltage activated calcium (calcium-L) (with maximal conductance $\bar{g}_{CaL}$); $I_{K,Ca}$, calcium-dependent potassium (with maximal conductance $\bar{g}_{K,Ca}$), I_L, leakage (with constant conductance g_L); I_{Kir}, opiod-activated, inwardly rectifying, voltage-dependent potassium (with maximal conductance $\bar{g}_{Kir}$); I_{KS}, 5-HT$_{1A}$R-dependent potassium (with maximal conductance $\bar{g}_{KS}$); I_{SynE}, excitatory synaptic (with conductance g_{SynE}); and I_{Syn_GABA} and I_{Syn_GLY}, GABAergic and glycinergic inhibitory synaptic currents (with conductances g_{GABA} and g_{Gly}), respectively.

Currents are described as follows:

$$\begin{aligned}
I_{Na} &= \bar{g}_{Na} \cdot m_{Na}^3 \cdot h_{Na} \cdot (V - E_{Na});\\
I_{NaP} &= \bar{g}_{NaP} \cdot m_{NaP} \cdot h_{NaP} \cdot (V - E_{Na});\\
I_K &= \bar{g}_K \cdot m_K^4 \cdot (V - E_K);\\
I_{CaL} &= \bar{g}_{CaL} \cdot m_{CaL} \cdot h_{CaL} \cdot (V - E_{Ca});\\
I_{K,Ca} &= \bar{g}_{K,Ca} \cdot m_{K,Ca}^2 \cdot (V - E_K);\\
I_L &= g_L \cdot (V - E_L);\\
I_{Kir} &= \bar{g}_{Kir} \cdot m_{Kir} \cdot (V - E_K);\\
I_{KS} &= \bar{g}_{KS} \cdot m_{KS} \cdot (V - E_K);\\
I_{SynE} &= g_E \cdot (V - E_{SynE});\\
I_{Syn_GABA} &= g_{GABA} \cdot (V - E_{Syn_GABA});\\
I_{Syn_Gly} &= g_{GLY} \cdot (V - E_{Syn_GLY}),
\end{aligned} \quad (2)$$

where E_{Na}, E_K, E_{Ca}, E_L, E_{SynE}, E_{Syn_GABA}, and E_{Syn_GLY} are the reversal potentials for the corresponding membrane and synaptic channels.

Variables m_i and h_i with indexes indicating ionic currents represent, respectively, the activation and inactivation variables of the corresponding ionic channels. Kinetics of activation and inactivation variables for all voltage-dependent currents except for I_{Kir} is described as follows:

$$\begin{aligned} \tau_{mi}(V) \cdot \frac{d}{dt} m_i &= m_{\infty i}(V) - m_i; \\ \tau_{hi}(V) \cdot \frac{d}{dt} h_i &= h_{\infty i}(V) - h_i. \end{aligned} \tag{3}$$

The expressions for steady-state activation and inactivation variables and time constants are shown in Table 1. Activation of calcium-dependent potassium channels (*K,Ca*) depends on the intracellular calcium concentration and is independent of voltage (see Table 1). Opioid-activated, inwardly rectifying voltage-dependent potassium (*Kir*) channels are activated if opioids are applied and remain inactivated otherwise. Because of the lack of specific data on the voltage dependency of channel kinetics, and for simplicity, the 5-HT_{1A}R-activated K^+ channels have been modelled as voltage-independent (leakage-type), drug concentration-dependent potassium (K_s) channels (see Appendix Table 1). The activation variable m_{KS} for these 5-HT_{1A}R-activated K^+ channels in the model depends only on the concentration (dose) of a 5-HT_{1A} receptor agonist (e.g. 8-OH-DPAT) applied (S). In all of our simulations, we consider S ≤ 5 μg/kg to be a low dose (at which m_{KS} is close to zero, i.e. the channels are almost closed) and S ≥ 10 μg/kg to be a higher dose, when these channels are activated (e.g. at 10 μg/kg, used in all of our simulations, m_{KS} = 0.5; see Appendix Table 1).

Table 1. Steady state activation and inactivation variables and time constants for voltage-dependent and other ionic channels

Ionic channels $m_\infty(V)$, V in mV; $\tau_m(V)$, ms; $h_\infty(V)$, V in mV; $\tau_h(V)$, ms
Fast sodium *Na* $m_{\infty Na} = 1/(1 + \exp(-(V + 43.8)/6))$; $\tau_{mNa} = \tau_{mNa\max}/\cosh((V + 43.8)/14)$, $\tau_{mNa\max} = 0.252$; $h_{\infty Na} = 1/(1 + \exp((V + 67.5)/10.8))$; $\tau_{hNa} = \tau_{hNa\max}/\cosh((V + 67.5)/12.8)$, $\tau_{hNa\max} = 8.456$
Persistent sodium *NaP* $m_{\infty NaP} = 1/(1 + \exp(-(V + 47.1)/3.1))$; $\tau_{mNaP} = \tau_{mNaP\max}/\cosh((V + 47.1)/6.2)$, $\tau_{mNaP\max} = 1$; $h_{\infty NaP} = 1/(1 + \exp((V + 60)/9))$; $\tau_{hNaP} = \tau_{hNaP\max}/\cosh((V + 60)/9)$, $\tau_{hNaP\max} = 4000$
Delayed rectifier potassium *K* $\alpha_{\infty K} = 0.01 \cdot (V + 44)/(1 - \exp(-(V + 44)/5))$; $\beta_{\infty K} = 0.17 \cdot \exp(-(V + 49)/40))$; $m_{\infty K} = \alpha_{\infty K}/(\alpha_{\infty K} + \beta_{\infty K})$; $\tau_{mK} = \tau_{mK\max}/(\alpha_{\infty K} + \beta_{\infty K})$, $\tau_{mK\max} = 1$
High-voltage activated calcium Ca_L $m_{\infty CaL} = 1/(1 + \exp(-(V + 27.4)/5.7))$; $\tau_{mCaL} = 0.5$; $h_{\infty CaL} = (1 + \exp((V + 52.4)/5.2))$; $\tau_{hCaL} = 18$
Calcium-dependent potassium *K,Ca* or *K(Ca^{2+})* $\alpha_{\infty K,Ca} = 1.25 \cdot 10^8 \cdot Ca^2$, $\beta_{\infty K,Ca} = 2.5$; $m_{\infty K,Ca} = \alpha_{\infty K,Ca}/(\alpha_{\infty K,Ca} + \beta_{\infty K,Ca})$; $\tau_{mK,Ca} = \tau_{mK,Ca\max} \cdot 1000/(\alpha_{\infty K,Ca} + \beta_{\infty K,Ca})$, $\tau_{mK,Ca\max} = 1 - 12$
Opiod-activated inwardly rectifying voltage-dependent potassium K_{ir} $m_{Kir} = k_O/(1 + \exp(-(V + 80)/5))$ k_O = 1 if opioids are applied, otherwise k_O = 0.
5-HT_{1A}R-activated potassium K_s $m_{KS} = 1/(1 + \exp(-([S] - thr)/2))$, thr = 10 μg/kg

The value of maximal conductances for all neuron types are shown in Appendix Table 2.

Table 2. Maximal conductances of ionic channels in different neuron types

Neuron type	$\bar{g}_{Na}$ (nS)	$\bar{g}_{NaP}$ (nS)	$\bar{g}_K$ (nS)	$\bar{g}_{CaL}$ (nS)	$\bar{g}_{K,Ca}$ (nS)	g_L (nS)	$\bar{g}_{Kir}$ (nS)	$\bar{g}_{KS}$ (nS)	$k_{\alpha 3}$
pre-I/I	170	4.0	180			2.5	14.0	1.2	0
early-I(1)	400		250	0.05	6.0	6.0	12.0	2.5	0
early-I(2)	400		250	0.05	6.0	6.0	12.0	1.2	1.7
post-I	400		250	0.05	6.0	6.0	5.0	2.3	0
dec-E	400		250	0.05	6.0	6.0	5.0	1.2	1.5
aug-E(1)	400		250	0.05	6.0	6.0	5.0	1.2	0.2
aug-E(2)	400		250	0.03	6.0	6.0	5.0	1.2	0
early-I(3)	400		250	0.07	6.0	6.0	5.0	1.2	0
ramp-I	400		250			6.0	5.0	1.2	0

The kinetics of intracellular calcium concentration Ca is described as follows (Rybak *et al.*, 1997a):

$$\frac{d}{dt} Ca = -k_{Ca} \cdot I_{CaL} \cdot (1 - P_B) + (Ca_0 - Ca)/\tau_{Ca}, \tag{4}$$

where the first term constitutes influx (with the coefficient k_{ca} and buffering (with the probability P_B), and the second term describes pump kinetics with resting level of calcium concentration Ca_0 and time constant τ_{Ca}.

$$P_B = B/(Ca + B + K), \tag{5}$$

where B is the total buffer concentration and K is the rate parameter.

The calcium reversal potential is a function of *Ca*:

$$E_{Ca} = 13.27 \cdot \ln(4/Ca) \quad (\text{at rest } Ca = Ca_o = 5.10^{-5}\text{mM} \text{ and } E_{Ca} = 150 \text{ mV}). \tag{6}$$

The excitatory (g_E) and the inhibitory GABAergic (g_{GABA}) and glycinergic (g_{GLY}) synaptic conductances are equal to zero at rest and may be activated by the corresponding synaptic input:

$$\begin{aligned} g_{Ei}(t) &= \bar{g}_E \cdot \sum_{j(E)} w_{ji} \cdot \sum_{t_{kj}<t} \exp(-(t - t_{kj})/\tau_E) + \bar{g}_d \cdot \sum_m w_{dmi} \cdot d_{mi}; \\ g_{GABAi}(t) &= \bar{g}_{GABA} \cdot \sum_{j(GABA)} w_{ji} \cdot \sum_{t_{kj}<t} \exp(-(t - t_{kj})/\tau_{GABA}), \\ g_{GLYi}(t) &= \bar{g}_{GLY} \cdot (1 + k_{\alpha 3} \cdot k_S) \cdot \sum_{j(GLY)} w_{ji} \cdot \sum_{t_{kj}<t} \exp(-(t - t_{kj})/\tau_{GLY}). \end{aligned} \tag{7}$$

In Eqn (7), each type of synaptic conductance for neuron i [the excitatory $g_{Ei}(t)$, inhibitory GABAergic $g_{GABAi}(t)$, and inhibitory glycinergic $g_{GLYi}(t)$] are summed over all inputs j of the corresponding type (indicated under the first sigma sign). The first equation in (7) for the excitatory synaptic conductances has a second term describing the integrated effect of inputs from m external drives d_{mi}. Each spike arriving at excitatory (E), or GABAergic (GABA) or glycinergic (GLY) neuron i from neuron j at time t_{kj} increases the corresponding synaptic conductance by $\bar{g}_E \cdot w_{ji}$, or $\bar{g}_{GABA} \cdot w_{ji}$, or $\bar{g}_{GLY} \cdot w_{ji}$, respectively, where $\bar{g}_E$, $\bar{g}_{GABA}$, and $\bar{g}_{GLY}$ are the parameters defining an increase in the corresponding synaptic conductance produced by one arriving spike at synaptic weight $w_{hy} = 1$. τ_E, τ_{GABA} and τ_{GLY} are the decay time constants for the corresponding conductances respectively. In the second term of the first equations, $\bar{g}_d$ is the parameters defining the increase in the excitatory synaptic conductance, respectively, produced by external input drive $d_{mi} = 1$ with a synaptic weight of $d_{im} = 1$. All drives were set equal to 1.

Table 3. Weights of synaptic connections in the network

Target population	Location	Excitatory drive {weight of synaptic input} or source population {type, weight of synaptic input from single neuron}
Pre-I/I	pre-BötC	Drive {1.17}; pre-I/I {E, 0.03}; dec-E {GLY, 0.15}; aug-E(1) {GABA, 0.1}
Early-I(1)	pre-BötC	Drive {2.1}; pre-I/I {E, 0.1}; dec-E {GLY, 0.25}; aug-E(1) {GABA, 0.4}; aug-E(2) {GABA, 0.05}
Early-I(2)	pre-BötC	Drive {0.7}; pre-I/I {E, 0.12}; post-I {GLY, 0.16}; dec-E {GLY, 0.22}; aug-E(1) {GABA, 0.35}; aug-E(2) {GLY, 0.05}
Post-I	BötC	Drive {1.7}; pre-I/I {E, 0.03}; early-I(2) {GLY, 0.24}; aug-E(1) {GABA, 0.165}; aug-E(2) {GLY, 0.165}
Dec-E	BötC	Drive {1.7}; early-I(1) {GABA, 0.1}; early-I(2) {GLY, 0.1}; aug-E(2) {GLY, 0.005}
Aug-E(1)	BötC	Drive {2.7}; early-I(1) {GABA, 0.15}; early-I(2) {GLY, 0.15}; dec-E {GLY, 0.25}
Aug-E(2)	BötC	Drive {1.5}; early-I(1) {GABA, 0.2}; dec-E {GLY, 0.25}
Early-I(3)	rVRG	Drive {3.5}; dec-E {GLY, 1.25}; aug-E(1) {GABA, 1.25}; aug-E(2) {GLY, 1.25}
Ramp-I	rVRG	Drive {5}; pre-I/I {E, 0.04}; early-I(3) {GLY, 1.25}; dec-E {GLY, 1.25}; aug-E(1) {GABA, 1.25}; aug-E(2) {GLY, 1.25}

Values in brackets represent relative weights of synaptic inputs from the corresponding drive (w_{dmi}) or source populations (type, w_{ji}); see Eqn (7). To provide heterogeneity of neurons within neural populations, the weights of excitatory and inhibitory connections were randomly distributed by ± 5% and ± 10%, respectively.

The effect of glycinergic synaptic input in the current model depends on the type of glycine receptors present in the neuron. We assume that all neurons have Glyα_1R mediating the inhibitory glycinergic synaptic input. In addition, we propose that some neural populations [specifically, the dec-E and aug-E(1) populations in the BötC and early-I(2) population in the pre-BötC; see Fig. 1B] contain an additional type of glycinergic α_3 receptors (Glyα_3R), which are co-expressed with the 5-HT$_{1A}$ receptors and can be activated by their agonists, such as 8-OH-DPAT. The latter if applied should produce a significant augmentation of the glycinergic inhibitory input to the neurons containing Glyα_3R. Correspondingly, the parameter k_S in Eqn (7) defines application of 8-OH-DPAT ($k_S = 1$ if 8-OH-DPAT is applied and zero otherwise); the parameter $k_{\alpha 3}$ defines the presence of Glyα_3R in a neuron ($k_{\alpha 3} \neq 0$, otherwise it is 0) and the density of this receptors that defines the degree to which the 5-HT$_{1A}$R-Glyα_3R complex increases the inhibitory effect of glycinergic input to the neuron ($k_{\alpha 3}$ values used can be found in Appendix Table 2).

The relative weights of synaptic connections (w_{ij} and d_{im} are shown in Appendix Table 3).

Neuronal parameters

Capacitance: C = 36 pF

Synaptic parameters: $\bar{g}_E = \bar{g}_{GABA} = \bar{g}_{GLY} = \bar{g}_d = 1.0$ ns; $\tau_E = 5$ ms, $\tau_{GABA} = \tau_{GLY} = 15$ ms. Differences in kinetics between GABA and glycine synaptic inputs have not been considered.

Calcium kinetics: $Ca_0 = 5{\cdot}10^{-5}$ mM; $k_{Ca} = 2{\cdot}10^{-5}$ mM/C; $\tau_{Ca} = 500$ ms, B = 0.030 mM; K = 0.001 mM.

Reversal potentials: $E_{Na} = 55$ mV; $E_K = -94$ mV; $E_{SynE} = -10$ mV; $E_{Syn\_GABA} = E_{Syn\_GLY} = -75$ mV.

To provide heterogeneity of neurons within neural populations, the value of E_L was randomly assigned from normal distributions using average value ± SD. Leakage reversal potential for all neurons (except for pre-I/I) $E_L = -60 \pm 1.2$ mV; for pre-I/I neurons $E_L = -68 \pm 1.36$ mV.

Modelling neural populations

In the present model, each functional type of neuron is represented by a population of 20–50 neurons. Connections between the populations were established so that, if a population A was assigned to receive an excitatory or inhibitory input from a population B or external drive D, then each neuron of population A received the corresponding excitatory or inhibitory synaptic input from each neuron of population B or from drive D, respectively. The heterogeneity of neurons within each population was set by a random distribution of E_L (mean values ± SD; see above) and initial conditions for values of membrane potential, calcium concentrations and channel conductances. In all simulations, initial conditions were chosen randomly from a uniform distribution for each variable, and a settling period of 20 s was allowed in each simulation before data were collected. Each simulation was repeated 20–30 times, and demonstrated qualitatively similar behaviour for particular values of the standard deviation of E_L and initial conditions.